Theoretical Aspects of Charge Ordering in Molecular Conductors

Hitoshi SEO[1]*, Jaime MERINO[2], Hideo YOSHIOKA[3], and Masao OGATA[4]

[1] *Non-Equilibrium Dynamics Project, ERATO-JST, c/o KEK, Tsukuba 305-0801, Japan*
[2] *Departamento de Física Teórica de la Materia Condensada, Universidad Autónoma de Madrid, Madrid 28049, Spain*
[3] *Department of Physics, Nara Women's University, Nara 630-8506, Japan*
[4] *Department of Physics, Faculty of Science, University of Tokyo, Tokyo 113-0033, Japan*

(Received February 4, 2008)

Theoretical studies on charge ordering phenomena in quarter-filled molecular (organic) conductors are reviewed. Extended Hubbard models including not only the on-site but also the inter-site Coulomb repulsion are constructed in a straightforward way from the crystal structures, which serve for individual study on each material as well as for their systematic understandings. In general the inter-site Coulomb interaction stabilizes Wigner crystal-type charge ordered states, where the charge localizes in an arranged manner avoiding each other, and can drive the system insulating. The variety in the lattice structures, represented by anisotropic networks in not only the electron hopping but also in the inter-site Coulomb repulsion, brings about diverse problems in low-dimensional strongly correlated systems. Competitions and/or co-existences between the charge ordered state and other states are discussed, such as metal, superconductor, and the dimer-type Mott insulating state which is another typical insulating state in molecular conductors. Interplay with magnetism, e.g., antiferromagnetic state and spin gapped state for example due to the spin-Peierls transition, is considered as well. Distinct situations are pointed out: influences of the coupling to the lattice degree of freedom and effects of geometrical frustration which exists in many molecular crystals. Some related topics, such as charge order in transition metal oxides and its role in new molecular conductors, are briefly remarked.

KEYWORDS: molecular conductors, charge ordering, strongly correlated electron system, low-dimensional systems, metal-insulator transition, superconductivity, magnetism, electron-lattice coupling, geometrical frustration

1. Introduction

The charge ordering (CO) phenomenon is actively studied in the research field of charge transfer type molecular conductors,[1] since it plays a key role in their physical properties. Following its clear observation in DI-DCNQI$_2$Ag,[2] metal-insulator transitions in many of these materials are now understood as due to CO. It has been found not only in newly synthesized compounds but also in systems which have been well known for years, where, however, its existence has been veiled until recently. Typical examples are two representative families of this field, the Bechgaard salts TM$_2X^3$ (TM = TMTSF or TMTTF) and ET$_2X^4$ (ET = BEDT-TTF) where X takes different atoms or molecules, both being studied for more than 20 years. The CO transition was revealed recently and now became one of the most important issues in these systems.

These materials are members of the so-called 2:1 salts expressed as A_2B, to which interest of this field has been conducted. Numerous compounds with such a 2:1 composition have been synthesized and found to exhibit a rich variety of properties.[5–7] Many of them show electron conduction at room temperature, where the carriers are due to a charge transfer from cations B^+ or anions B^-, resulting in an average valence of $-1/2$ or $+1/2$ for A molecules, respectively. The B ion has closed shell in most cases then the valence band near the Fermi energy is composed of the frontier orbital, LUMO or HOMO, of the A molecule, which is quarter-filled as a whole in terms of electrons or holes. The variety in their properties has been revealed to be originated from the diversity of anisotropic lattices resulting in different non-interacting band structures, together with strong correlation effects experienced by electrons among this HOMO/LUMO band determining the low energy properties.[8] CO is a typical consequence of such strong correlation, namely, large electron-electron Coulomb repulsion compared to the kinegic energy, especially due to the long-range nature of this Coulomb force. In fact, it is now ubiqitously found in A_2B compounds as well as in other strongly correlated electron systems such as transition metal oxides.

In this article, we review theoretical aspects of CO mainly aiming at following points: In what kind of situation are they formed? In what situation do they melt? How does the spin degree of freedom act? Are there any superconducting (SC) state near the CO phase?

Such theoretical works on CO have been done from early days, motivated by experiments. For example, the metal-insulator transition in a classical transition metal oxide Fe_3O_4, the magnetite, was proposed to be due to CO by Verwey,[9] although its existence is still controversial to date.[10] Another trigger was an early molecular conductor TTF-TCNQ, where an incommensurate $4k_F$ charge-density-wave (CDW) is observed, but only in a diffusive manner therefore long ranged order is not achieved.[11,12] Here we refer to the term CO as the phe-

*E-mail address: seo@post.kek.jp

nomenon due to strong Coulomb interaction, sometimes called as "Wigner crystal on lattice".[13] This should be distinguished with other transitions resulting in periodic modulations of the charge density, such as the $2k_F$ CDW (the Peierls-Frölich state) driven by the nesting of the Fermi surface together with the electron-lattice coupling,[12] which is essentially a phenomenon at weak correlation.

The observations of CO transition in A_2B molecular systems have stimulated many theoretical studies adhered to these compounds. Experiments have fortunately appeared around when researchers in this field started to realize that effects of electron correlation could be modeled in a straightforward way and that rather simple models would successfully describe their physical properties.[14] That is, each constituent A molecule is represented by a "site" and only the frontier orbital is considered. The non-interacting band structures near the Fermi level are well reproduced by the extended Hückel tight-binding scheme.[15,16] Then, the Coulomb interaction between electrons in this orbital is taken into account.[17,18] We call such model as the extended Hubbard model (EHM), written as follows:

$$\mathcal{H}_{\rm EHM} = -\sum_{\langle ij\rangle\sigma}\left(t_{ij}c^{\dagger}_{i\sigma}c_{j\sigma}+h.c.\right) + \sum_i U n_{i\uparrow}n_{i\downarrow} + \sum_{\langle ij\rangle} V_{ij}n_i n_j. \quad (1)$$

Here, $\langle ij\rangle$ denotes pairs of the lattice sites (i.e., molecules) i and j, σ is the spin index which takes $\uparrow$ and $\downarrow$, $n_{i\sigma}$ and $c^{\dagger}_{i\sigma}$ ($c_{i\sigma}$) denote the number operator and the creation (annihilation) operator for the electron of spin σ at the ith site, respectively, and $n_i = n_{i\uparrow} + n_{i\downarrow}$. The transfer integrals, t_{ij}, reflect the anisotropy resulting from the particular spatial extent of the frontier orbital, calculated, e.g., by the extended Hückel method or from tight-binding fitting of first principle calculations. The Coulomb interactions of not only on-site U but also intersite V_{ij} are considered, the latter being crucial for the CO as we will see later explicitly. In the $[A_2]^-B^+$ ($[A_2]^+B^-$) systems the non-interacting band as a whole is quarter-filled in terms of electrons (holes), namely, there exists one electron (hole) per two sites on average.

Because of this clear way of constructing microscopic models from crystal structures, results of theoretical works could be checked back in the experiments, and such interplay has greatly accelerated the research. Throughout these we have learned that, although the basic picture of CO is rather classical and essentially known from the early days, the physics therein is rich and diverse. The main reason for such diversity is the variety in the geometry of lattice structures of the materials where it is realized. More specifically, relative positions between molecules not only reflect directly on the anisotropy in t_{ij} controlling the band structure, but also affect drastically the nature of the CO state itself through V_{ij}. This is in contrast with the case of the Mott insulating state in half-filled systems where the driving force is the on-site term U, which is a character of the atom/molecule itself; in the case of the dimer-type Mott insulator in A_2B systems (see later), it is the "on-dimer" Coulomb repulsion, $U_{\rm dimer}$.[17,19,20]

The research of CO is still continuing and rather rapidly growing. New phenomena are uncovered, even in the above mentioned compounds, and now under extensive investigations. For example a pressure-temperature phase diagram of DI-DCNQI$_2$Ag has been explored where an anomalous temperature dependence of metallic resistivity $\rho \propto T^3$ is found just beyond the border of the CO phase.[21] A peculiar interplay between CO and magnetic properties found in TMTTF$_2X$ compounds under pressure[22] requires a reformulation of the generic phase diagram of TM$_2X$.[23] Problems of CO system on anisotropic triangular lattice structures characteristic of ET$_2X$ compounds have many new aspects.[4,24] We cannot offer comprehensive explanation for each of these cases here as many are still not yet resolved theoretically, but we hope that this review, by explaining the present status, would provide a base for tackling such new physics and lead the readers toward challenges.

The organization of this paper is as follows. Since most of the A_2B compounds have low-dimensional structures, we will devide this review into one-dimensional (1D) and two-dimensional (2D) problems, while in reality there exist finite interchain/interlayer interactions; they are quasi-1D and quasi-2D systems. Theoretical results devoted for the quasi-1D compounds are described in § 2. This starts with studies on purely 1D electronic models and then additional effects, such as interchain interaction and coupling to the lattice degree of freedom, are considered. The 1D case can be studied in more controlled ways, analytically and numerically, than in the study of the quasi-2D compounds, which we discuss in § 3. There, theoretical works on 2D electronic models are still in progress and influence of additional effects, e.g., coupling to the lattice, is not fully understood yet. Studies aimed at SC states near the CO phase in 2D models, motivated by its observations, are reviewed as well. A problem of CO systems under geometrical frustration which is expected to be relevant to many molecular conductors will be pointed out in § 2 and 3. In § 4 related topics will be mentioned, such as analogous CO states observed in transition metal oxides. Possible roles of CO in other molecular systems will be added as well, as perspectives. A summary is given in § 5.

Some of the experimental studies on CO are mentioned in this review but many references including important ones are left out; we refer to other reviews from experimental standpoints[1,25] which would be complementary to this article. One can find many review articles on the properties of molecular compounds in general,[1,5–7] especially we refer to refs. 8 and 18 for papers from theoretical but more systematic point of views including the CO systems as well.

2. Quasi-One-dimensional Systems

Early theoretical works on CO in 1D models have been performed motivated by the observation of $4k_F$ CDW in TTF-TCNQ as mentioned in § 1, where the importance of the long-range Coulomb interaction was empha-

sized.[13,26–30] However for the quasi-1D A_2B systems, before CO was found, analyses were mainly concentrated on the Hubbard-type models only considering the on-site Coulomb energy U, but some did discuss the relevance of the inter-site V_{ij}.[31–33] For example, Mila[33] estimated that the nearest-neighbor Coulomb repulsion is appreciable in TM_2X, such as more than one third of U, by comparing calculations on the dimerized version of 1D EHM (see eq. (2)) with optical measurements.[34] After CO was found, many further works devoted to the 1D EHM and its variants have been carried out, which we will review in this section.

2.1 *Charge ordering in quasi-one-dimensional systems*

When the first observation of CO in DI-DCNQI$_2$Ag was made by ^{13}C-NMR,[2] in an independent theoretical work based on mean-field (MF) approximation, Seo and Fukuyama[35] proposed that CO due to the nearest-neighbor Coulomb repulsion might exist in TMTTF$_2X$. This was based on a comparison between self-consistent solutions at zero temperature obtained by the standard MF treatment applied to the appropriate dimerized 1D EHM and the spin structure in the antiferromagnetic phase suggested by a ^{1}H-NMR measurement.[36] Soon after, it was found that members of TMTTF$_2X$ indeed show CO, directly seen in a ^{13}C-NMR measurement.[3] Moreover a divergence of the dielectric constant at the CO transition temperature is observed, suggesting a ferroelectric state.[37] This is a consequence of CO, which we will mention later in this section.

These systems are members of DCNQI$_2X$ (X: monovalent metal cation X^+, e.g., Ag and Li)[38,39] and TM_2X (X: monovalent anion X^-, e.g., PF$_6$, AsF$_6$, SCN, and Br),[23] respectively, both having quasi-1D structures. DCNQI stands for the R_1R_2-DCNQI molecule where R_1, R_2 are sustituents such as CH$_3$, Br, I, etc. Here, quasi-1D "structure" implies twofold meanings: in their crystal structures the DCNQI/TM molecules assemble in a stacking manner, and, in their electronic structures the transfer integrals in the interchain direction, $t_{\rm inter}$, are one order of magnitude smaller than those in the intrachain direction, $t_{\rm intra}$.

The networks of DCNQI/TM molecules are schematically shown in Fig. 1. In DCNQI$_2X$ the interchain couplings are three-dimensional (3D) and uniform, while TM_2X they are quasi-2D and the TM molecules are connected in a rather complicated way (the β-type structure; see § 3.1). For DCNQI$_2X$ systems, $|t_{\rm intra}| \simeq 0.15 \sim 0.25$ eV, $|t_{\rm inter}| \simeq 0.01 \sim 0.03$ eV,[40,41] while for TM_2X systems: in TMTSF compounds $|t_{\rm intra}| \simeq 0.2 \sim 0.4$ eV, $|t_{\rm inter}| \simeq 0.01 \sim 0.05$ eV and in TMTTF compounds $|t_{\rm intra}| \simeq 0.1 \sim 0.25$ eV, $|t_{\rm inter}| \simeq 0.01 \sim 0.03$ eV.[16,42–44] These values depend on the actual salts and different methods of calculation also provide varied estimations.

We note that the distances between molecules does not simply correspond to the degree of anisotropy in t_{ij}, since the anisotropic shape of the frontier orbitals makes the dependence of t_{ij} to the relative configuration of molecules rather complicated in general.[16,45] In contrast, V_{ij} obeys more or less a monotonic function of the distance because it is the Coulomb interaction. Therefore the interchain part of V_{ij} is not necessarily small compared to the intrachain one even in these quasi-1D systems.[46,47] However, let us neglect the interchain interactions first and discuss this issue later in § 2.4 and 2.6.

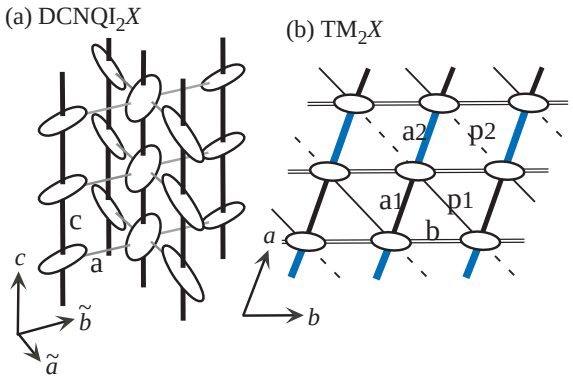

Fig. 1. (Color online) Schematic representation of the molecular networks in (a) DCNQI$_2X$ and (b) TM_2X. The crystallographic axes are shown; in (a) we take $\tilde{a} = a + b$, $\tilde{b} = a - b$ where a and b are the axes in the tetragonal cell. The interchain interactions are three-dimensional in (a), whereas it is two-dimensional in (b) since interlayer couplings are one order of magnitude smaller due to the anion layers. The indices (for TM_2X, taken from ref. 16) are not only for t_{ij} but also for different values of V_{ij}, although the degree of anisotropy can be different (see text).

Estimations of the Coulomb energies in these molecular systems are difficult at present. Quantum chemistry calculations are performed for an isolated molecule or clusters of them, which provide unrealisticly large values since the screening effect in solids is left out, while such estimations from the first principle in these molecular solids are still yet to be done. However it is believed to be of the order of $U \simeq 1$ eV from different measurements and estimates, which gives $U/|t_{\rm intra}| \simeq 5$ for DCNQI$_2X$ and TMTTF$_2X$, while for TMTSF$_2X$ smaller values of $U/|t_{\rm intra}| \simeq 3$. The estimated values for the intrachain Coulomb energy $V_{\rm intra}$ are again ambiguous but many provide rather large values: the ratio $V_{\rm intra}/U$ in a range about $0.2 \sim 0.6$.[33,46–48]

A crucial difference between these two families is that the stacking of DCNQI molecules is uniform while that of TM moluecules is slightly dimerized, as seen in Fig. 1. Thus a minimal effective model to investigate the occurance of CO in these compounds is the 1D dimerized EHM, represented as,

$$\mathcal{H}_{\rm 1D} = -t\sum_{i\sigma}(1+(-1)^i\delta_{\rm d})(c^\dagger_{i+1\sigma}c_{i\sigma} + h.c.) + U\sum_i n_{i\uparrow}n_{i\downarrow} + V\sum_i n_i n_{i+1}, \qquad (2)$$

where i is the site index along the chain. Here, the transfer integrals allow dimerization as alternating $t(1+\delta_{\rm d})$ and $t(1-\delta_{\rm d})$; in the DCNQI compounds $\delta_{\rm d} = 0$, while for the TM compounds values of t_{a1} and t_{a2}[16,42–44] (for the indices see Fig. 1) read $\delta_{\rm d} \lesssim 0.1$. The inter-site Coulomb repulsion between neighboring sites is set to be uniform as V, which is an approximation for TM_2X. Again, the value of $\delta_{\rm d}$ does not directly result in a similar value of dimerization in $V_{\rm intra}$. In fact, quantum chemistry calcu-

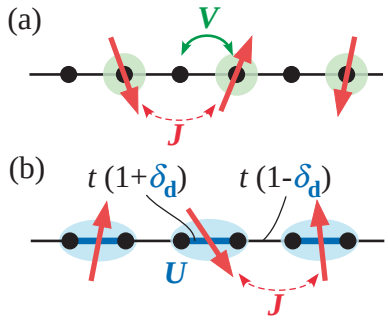

Fig. 2. (Color online) Two limiting cases of strongly correlated insulators in quarter-filled system[8,18] : (a) the charge ordered insulating state and (b) the dimer Mott insulating state. Black dots and colored area represent the lattice sites and the localized carriers, respectively, while the thickness of the bonds show the difference in the transfer integrals. The arrows show the paramagnetic localized spins.

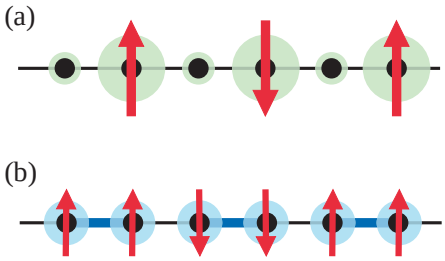

Fig. 3. (Color online) Typical mean-field solutions in one-dimensional dimerized extended Hubbard model at quarter-filling,[35] $\mathcal{H}_{1D}$ in eq. (2): (a) the charge ordered antiferromagnetic insulating state for $\delta_d = 0$ and large U and V, and, (b) the dimer-type antiferromagnetic insulating state for $\delta_d \neq 0$, large U, and $V = 0$. The size of the colored circles and the arrows represents the charge density and the amount of spin moment on each site. The charge densities are (a) disproportionated alternatively as, $1/2+\delta$, $1/2-\delta$, $1/2+\delta$, $1/2-\delta$, where δ is the amount of charge disproportionation, and (b) uniform at 1/2.

lations for TM_2X[46,47] provide the dimerization parameters in V_{a1} and V_{a2} to be less than 1 %. For the DCNQI compounds the electron filling is one quarter while it is three quarter for the TM compounds, but in this 1D model the two situations are equivalent since electron-hole symmetry holds. Note that other effects may break this symmetry then we should treat the two cases separately.

It is useful to describe two limiting cases for the insulating states in this model at quarter-filling due to strong Coulomb interaction,[8,18] which are shown in Fig. 2. These states, in a broad sense, are realized in a wide range of A_2B compounds, not only in quasi-1D but also in quasi-2D systems discussed in § 3. One is the Wigner crystal-type CO state stabilized by V in the presence of strong U, and the other is the Mott insulating state stabilized by U in the presence of strong dimerization δ_d: a dimer Mott insulator. The spin degree of freedom in such insulating states would behave as an $S = 1/2$ localized spin chain, where the spins are located on every other site for the CO state whereas on every dimer for the dimer Mott insulating state. Roughly speaking, charge localization is determined by large energy scales such as U and V, while spin properties are determined by a smaller energy scale of the order of the Heisenberg coupling, J, acting between these localized spins. We will discuss their detailed properties in the following subsections.

The MF solutions mentioned above are consistent with such two limiting cases. This is seen in the obtained spin and charge patterns for the two cases, schematically shown in Fig. 3, and actually many works have been performed on $\mathcal{H}_{1D}$ based on such MF results.[49] However we should keep in mind that this MF treatment cannot correctly describe such insulators at strongly correlated regime in general, for example the paramagnetic insulating phase at temperatures above the magnetically ordered phases observed in experiments cannot be reproduced. Moreover in purely 1D models the role of quantum fluctuations which is left out in MF is crucial, and we will see that it considerably modifies the MF results.

We note that the cations/anions are at crystallographically equivalent positions from the DCNQI/TM molecules at high temperatures so that, essentially, they do not contribute to the electronic properties. However, in the case of non-centrosymmetrical anions in TM_2X, the anions show a disorder-to-order transition by lowering temperature and generate a potential with longer periodicity than the original unit cell, resulting in modifications in the one-particle properties.[50] We do not discuss such cases in this paper since its relation with the CO due to electron correlation is still obscure, but the fact that the anion ordering produces charge density modulations suggests the importance of the anions in some cases. Actually possible roles of the X unit in stabilizing CO states through its coupling to the electron system will be addressed in § 2.5.

2.2 *One-dimensional extended Hubbard model*

The quarter-filled 1D EHM, $\mathcal{H}_{1D}$ in eq. (2) with δ_d=0, was first considered by Ovchinnikov[26] who discussed that in the $U/t = \infty$ limit a CO insulating ground state is realized for $V > 2t$ ($= V_{cr}$), as in the following. In this limit, double occupancy is strictly prohibited so that every site is either occupied or unoccupied. Furthermore the spin degree of freedom is frozen since the "order" of electrons cannot be changed due to the 1D nature. Then the charge degree of freedom is equivalent to a spinless fermion (SF) model at half-filling with the nearest neighbor Coulomb interaction V, i.e., the interacting SF model, and the spin degree of freedom acts freely as Curie spins.

This SF model, by identifying occupied site as up spin and unoccupied site as down spin, can be mapped onto a 1D $S = 1/2$ (pseudo-)spin model through Jordan-Wigner transformation. Quarter-filling in the original electronic system corresponds to half-filling in the SF model where half of the sites would be occupied, and to total magnetic moment of zero in the effective spin model. The inter-site Coulomb interaction between SF transforms to an antiferromagnetic interaction, $J_z S_i^z S_j^z$ with $J_z = V$, while the kinetic enery term becomes as $J_{xy}(S_i^x S_j^x + S_i^y S_j^y)$ with $J_{xy} = 2t$. This is an XXZ model, where a $T = 0$ phase transition from a gapless "XY" state ($J_z < J_{xy}$) to an antiferromagnetic "Ising" state ($J_z > J_{xy}$) is known.[51] Transforming back to the SF model, these correspond to a metallic Tomonaga-Luttinger liquid (TLL) and the CO insulating state, repectively; the critical point is the

Heisenberg point $J_{xy} = J_z$, i.e., $V = V_{\rm cr}$.

It is noteworthy that this is in fact a rigorous demonstration of a "classical" picture of CO discussed in systems regardless of the dimension.[52] In general, the CO problem, in the condition of kinetic energy set to 0 ($t_{ij} = 0$) in addition to infinite U with no double occupancy discussed above, can be described by SF's interacting only by the inter-site Coulomb repulsion V_{ij}. This can be mapped onto Ising models, $J_{ij}\sigma_i\sigma_j$, with $J_{ij} = V_{ij}$, similarly to the J_z-term in the 1D case above. Therefore, analogies between spin systems and CO systems can be generally expected in the presence of strong correlation, although the mapping is only approximate for 2D and 3D systems with finite t_{ij} and U, and even for 1D systems with finite U.

Since the charge and spin degrees of freedoms are completely decoupled in the $U/t = \infty$ limit, the ground state wave function has the form $|\Phi\rangle = |\phi_{\rm SF}\rangle|\chi_\sigma\rangle$, where $|\phi_{\rm SF}\rangle$ is the ground state of SF's and $|\chi_\sigma\rangle$ denotes the spin configuration. On the other hand, at finite U/t, these spins interact with each other. In the large-U region, recently Tanaka and Ogata[53] analytically discussed the V-dependence of the magnetic susceptibility χ. This is done by extending the large-U studies of the 1D Hubbard model based on the Bethe ansatz,[54,55] where the charge degree of freedom can be represented by SF's, and the spin degree of freedom is described by Heisenberg spin chains with an effective exchange coupling $J_{\rm eff}$. For the 1D EHM, according to the degenerate perturbation theory,[55] the degeneracy of the spin system is lifted by a term proportional to $J = 4t^2/U$. However, because of the presence of the charge degree of freedom, $J_{\rm eff}$ is not just equal to J, but also depends on the probability of finding two SF's on nearest-neighbor sites, namely, $\langle n_i n_{i+1}\rangle_{\rm SF} \equiv \langle\phi_{\rm SF}|n_i n_{i+1}|\phi_{\rm SF}\rangle$. (There is another contribution to $J_{\rm eff}$ discussed in ref. 53.) This value decreases as V increases and its derivative with respect to V is continuous even at $V_{\rm cr}/t$,[51] where the CO transition occurs. This is because the phase transition is a Berezinskii-Kosterlitz-Thouless (BKT) type,[56,57] which is essentially different from either first or second order transition. The divergence of the correlation length is more rapid than any power law, and then the gap increases very slowly near the critical point: the charge gap behaves as $\Delta_{\rm c} \simeq 4\pi\exp(-\pi^2/2(2(\rho-1))^{\frac{1}{2}})$,[53,58] with $\rho = V/2t \geq 1$. Reflecting these, χ increases as a monotonic function of V since χ is proportional to $1/J_{\rm eff}$,[54,55] continiously through the CO transition point (see also Fig. 5). This indicates that the fluctuation is large near the phase boundary even in the CO states, and consequently CO has small effect on the spin degree of freedom.

For whole finite values of U and V, Mila and Zotos[31] first provided the ground state phase diagram on the plane of U/t and V/t, using numerical Lanczos exact diagonalization (ED) method[59] for finite size systems up to $L = 16$ sites. They have judged the metal-insulator phase boundary by calculating the charge gap for finite systems as $\Delta_{\rm c} = [E_0(L/2+1) + E_0(L/2-1) - 2E_0(L/2)]/2$, where $E_0(n)$ is the ground state energy for n electron system ($n = L/2$ for quarter-filling), and extrapolating

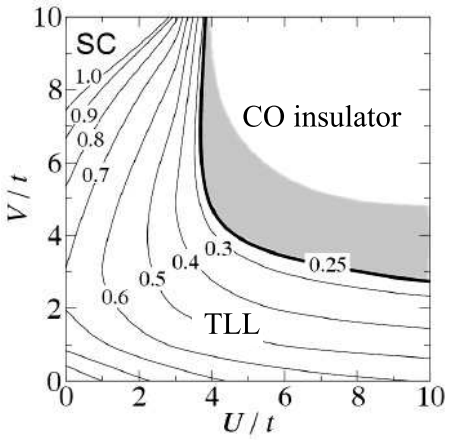

Fig. 4. Ground state phase diagram of the one-dimensional extended Hubbard model at quarter-filling on the plane of U/t and V/t.[63] CO stands for charge order and TLL for Tomonaga-Luttinger liquid. SC represents the superconducting phase. Contour map for the Tomonaga-Luttinger parameter K_ρ is shown. The bold line represents the boundary for the metal-insulator transition. The shaded area is the region with an exponentially small gap. [By courtesy of S. Ejima.]

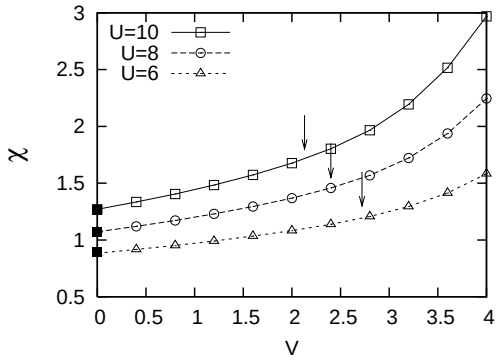

Fig. 5. Spin susceptibility χ calculated by exact diagonalization as a function of V for several values of U at quarter filling ($t = 1$).[53] Solid squares represent exact results in the one-dimensional Hubbard model and arrows indicate the points above which the charge gap opens. [After ref. 53.]

the results to the thermodynamic limit. Later, different numerical methods have been applied by different authors[32,60–63] and the main features are confirmed; the phase diagram by Ejima *et al.*[63] is shown in Fig. 4, which is determined by the density matrix renormalization group (DMRG) method treating system sizes up to more than $L = 100$ sites. The CO insulating state is in the large $(U/t, V/t)$ region, while the metallic state in the rest is the TLL. The TLL parameter K_ρ, which is the exponent characterizing the power of the correlation function, becomes equal to $K_\rho = 1/4$ at the phase boundary ($K_\rho = 1$ at $U = V = 0$). As U is increased, this phase boundary approaches to $(U/t = \infty, V/t = 2)$, the exact value explained above.

The magnetic susceptibility χ has been discussed in ref. 53 for such finite $(U/t, V/t)$. This is done numerically by the Lanczos ED method up to $L = 16$ sites, as shown in Fig. 5 where χ at $T = 0$ for several values of U/t and V/t are plotted. The TLL property $\chi = 2/\pi u_\sigma$ is used with u_σ being the velocity of the spin excitation (i.e., the spin velocity).[64] The critical values for the metal-CO insulator transition are indicated by arrows in

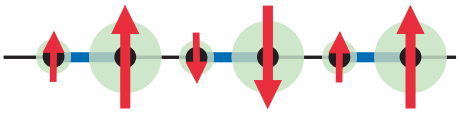

Fig. 6. (Color online) Coexistence of charge order and dimerization in the one-dimensional dimerized extended Hubbard model for TM_2X. This is a schematic drawing of the mean-field solution, where antiferromagnetism also coexists.[35] Charge disproportionation exists as in the charge ordered state in Fig. 3 (a) whereas the amount of spin moment, parallel whithin dimers and antiparallel between them, are also disproportionated in a similar way.

Fig. 5. One can see that χ increases with V, namely, $J_{\rm eff}$ is suppressed as in the large-U case above. χ smoothly varies as a function of V even through the CO phase transition, as in the exact calculation in the large-U case.[53] The spin susceptibility is again not affected much by the opening of a charge gap. This is consistent with field theoretical studies that we will see in § 2.3, indicating the transition to be of the BKT type for finite $(U/t, V/t)$ as well.

In the presence of finite dimerization $\delta_{\rm d}$, it has been well known for the $V = 0$ case, namely, the 1D dimerized Hubbard model, that $\delta_{\rm d}$ together with U always give rise to the dimer Mott insulating state (Fig. 2(b)) for quarter-filling. This is because $\delta_{\rm d}$ opens an energy gap at $\pm 2k_{\rm F}$ in the non-interacting energy dispersion making the lower band effectively half-filled. Then even for an infinitesimal repulsion the system becomes a Mott insulator which is characteristic of 1D half-filled electronic systems. This situation have been theoretically investigated extensively,[65] from the large-U case[66,67] to the small-U case.[68] When finite V is added, there arises a competition between two insulating states, this dimer Mott insulator and the CO insulator.[35] The CO state here can be considered as a coexistence of dimerization and CO as seen in Fig. 6. Accurate numerical calculations are yet to be done and now in progress,[33,69–71] so let us discuss such competition in the next subsection.

2.3 Bosonization

The bosonization method is one of the most powerful tools to treat 1D systems analytically.[72] In this approach, quantum fluctuation, which plays an essential role on the electronic state in 1D systems, can be fully taken into account, in contrast to the MF theory. Furthermore, the analytical treatment enables us to capture insight of the physics, e.g., found in numerical calculations discussed in the previous subsection. It has been successfully applied to $\mathcal{H}_{\rm 1D}$ in eq. (2) by Yoshioka *et al.*,[73,74] as in the following, who clarified the relation between such lattice models and the conventional "g-ology" picture.

In the ordinary bosonization procedure, only the one-particle fermion states around the two Fermi wavenumber, $\pm k_{\rm F}$, are considered and the four body interaction in the Hamiltonian is expressed in terms of these states. In quarter-filled systems, the $8k_{\rm F}$-Umklapp scattering exists[75–78] because of $k_{\rm F} = \pi/(4a)$ with a being the lattice spacing and it is crucial for the appearance of the insulating state. However, one can not obtain this Umklapp scattering by the ordinary method above. This is because it can only be expressed by the interaction processes where four right-going electrons are scattered into the left-going states and vice versa to gain (or loose) $8k_{\rm F}$, and then the scattering should include higher order interaction processes through the one-particle state around $\pm 3k_{\rm F}$.

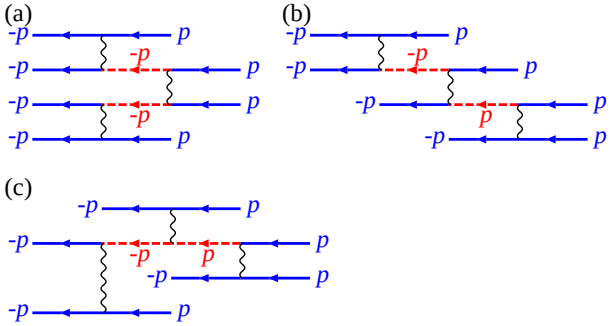

Fig. 7. (Color online) Diagrams representing the $8k_{\rm F}$-Umklapp scattering. Here $p = +/-$ expresses the right/left-going one-particle states and the solid and the dotted lines express the electrons near $\pm k_{\rm F}$ and $\pm 3k_{\rm F}$, respectively.

A systematic way to derive the $8k_{\rm F}$-Umkpapp scattering has been developped[73,74] as follows. The one-particle states are divided into two parts: the states near $\pm k_{\rm F}$ and those near $\pm 3k_{\rm F}$. The effective Hamiltonian written in terms of the former states near $\pm k_{\rm F}$ is obtained by integrating out the one-particle states near $\pm 3k_{\rm F}$ and treating the interaction processes including both the states near $\pm k_{\rm F}$ and those near $\pm 3k_{\rm F}$ perturbatively. The $8k_{\rm F}$-Umklapp scattering appear in the third order interaction processes shown in Fig. 7.

Then we can express the effective phase Hamiltonian for the 1D EHM with $\delta_{\rm d} = 0$, by using the bosonic phase variables representing the charge and spin fluctuations.[79] The Hamiltonian is divided into the charge part, $\mathcal{H}_\rho$, and the spin part, $\mathcal{H}_\sigma$, which is essentially the same as that of the 1D isotropic Heisenberg model with a gapless excitation. $\mathcal{H}_\rho$ is given by the sine-Gordon model shown below,

$$\mathcal{H}_\rho = \frac{v_\rho}{4\pi}\int {\rm d}x \left\{ \frac{1}{K_\rho}(\partial_x\theta_\rho)^2 + K_\rho(\partial_x\phi_\rho)^2 \right\} + \frac{g_{1/4}}{2(\pi\alpha)^2}\int {\rm d}x \cos 4\theta_\rho, \tag{3}$$

where $[\theta_\rho(x), -\partial_{x'}\phi_\rho(x')/(2\pi)] = {\rm i}\delta(x-x')$, and v_ρ and K_ρ are the velocity of the charge excitation and the TLL parameter introduced in § 2.2, respectively. The quantity α^{-1} is the ultraviolet cutoff of the order of a^{-1}.

The coefficient of the non-linear term $g_{1/4}$ expressing the $8k_{\rm F}$-Umklapp scattering is written as, $g_{1/4} = (Ua)^2(Ua - 4Va)/8(\pi t\alpha)^2$. The order parameter of CO at the i-th site, $O_{\rm CO}(x_i)$ is given by using the phase variables, as $O_{\rm CO}(x_i) \propto \cos(4k_{\rm F}x_i + 2\theta_\rho) = (-1)^i \cos 2\theta_\rho$, where $x_i = ia$. This indicates that CO is stabilized for $\theta_\rho = 0$ and $\theta_\rho = \pi/2$, whereas it disappears for $\theta_\rho = \pi/4$ and $\theta_\rho = 3\pi/4$. The former and the latter can be realized in the case of $g_{1/4} < 0$ and $g_{1/4} > 0$, respectively. This shows explicitly the fact that the inter-site Coulomb repulsion V stabilizes the CO state through the decrease of $g_{1/4} < 0$ as V is increased. We note that this condition $g_{1/4} < 0$ for the appearance of CO, i.e., $4V > U$, is also a necessary condition

in the MF treatment. This is based on the charge susceptibility within random phase approximation (RPA) , $\chi_c(q) = \chi_0(q)/[1 + (U + 4V\cos qa)\chi_0(q)]$, where $\chi_0(q)$ is the noninteracting charge susceptibility taking a positive value; $4V > U$ is required for χ_c to diverge at $qa = \pi$, i.e., for the realization of the CO state with $q = 4k_F$.

The low energy property of the phase Hamiltonian $\mathcal{H}_\rho$ is determined by the renormalization group equations by introducing $l = \ln(\alpha'/\alpha)$ with a new scale α' ($> \alpha$),

$$\frac{\mathrm{d}}{\mathrm{d}l}K_\rho(l) = -8G_{1/4}(l)^2K_\rho(l)^2, \tag{4}$$

$$\frac{\mathrm{d}}{\mathrm{d}l}G_{1/4}(l) = (2 - 8K_\rho(l))G_{1/4}(l). \tag{5}$$

The initial conditions are $K_\rho(0) = K_\rho$ and $G_{1/4}(0) = g_{1/4}/(2\pi v_\rho)$. Whether the system is in the metallic TLL state or in the CO insulating state is determined by the $l \to \infty$ solutions characterized by $G_{1/4}(\infty) = 0$ or $G_{1/4}(\infty) = -\infty$, respectively. The phase boundary determined by the renormalization group equations, where $K_\rho(\infty) = 1/4$, is shown by the dotted curve in Fig. 8 where $\alpha = 2a/\pi$ is used. This phase transition is of BKT type since the sine-Gordon theory is equivalent to the low-energy properties of the classical 2D XY model. The phase diagram obtained by the present bosonization theory is qualitatively the same as that shown in Fig. 4.

The bosonization theory above can be straightforwardly extended to include the dimerization δ_d together with finite V.[80] As a result of the energy gap at $\pm 2k_F$ in the non-interacting energy dispersion due to finite value of δ_d, in addition to $\mathcal{H}_\rho$ in eq. (3), the $4k_F$-Umklapp scattering is generated.[68] This is expressed in terms of the phase variables as,

$$\mathcal{H}_{1/2} = -\frac{g_{1/2}}{2(\pi\alpha)^2}\int \mathrm{d}x \sin 2\theta_\rho, \tag{6}$$

where $g_{1/2}$ is proportional to δ_d for $|\delta_d| \ll 1$. The ground state phase diagram in the presence of δ_d determined by the renormalization group equations, on the plane of V/t and U/t, is shown in Fig. 8. Due to the $4k_F$-Umklapp scattering, the metallic TLL state changes to the dimer Mott insulating state with uniform charge distribution even for infinitesimal interactions, as expected from the works for $V = 0$.[65] The CO insulating state (Fig. 6) is suppressed because the commensurability energies due to the two kinds of Umklapp scattering compete with each other for $g_{1/4} < 0$ and $\mathcal{H}_{1/2}$ has a larger scaling dimension. Nevertheless, importantly, the CO phase still exists in the large $(U/t, V/t)$ region. This model for the charge sector having two non-linear terms is called the double frequency sine-Gordon model and it is suggested that the phase boundary between the dimer Mott insulator and the CO insulator is an Ising type phase transition, where the charge gap Δ_c becomes 0 at the phase boundary.[71,81]

2.4 Interchain coupling

In purely 1D systems, phase transitions do not occur at finite temperatures because any ordered state collapses due to thermal fluctuations. In this sense, the critical temperature for CO, T_{CO} in the 1D EHM that we have discussed in § 2.2 and 2.3 is always absolute zero temperature. However, quasi-1D materials such as $DCNQI_2X$ and TM_2X undergo phase transitions at finite temperatures, which is a consequence of the three (or two) dimensionality. In the electronic sector, there exist two kinds of interchain couplings; one is the single particle hopping between the chains (t_{inter}) and the other is the mutual Coulomb interaction between electrons in different chains (V_{inter}). As mentioned in § 2.1, t_{intra}/t_{inter} is of the order of 10 in the DCNQI and TM salts, while the interchain V_{inter} may be of the same order with the intrachain V_{intra}. There are quantum chemistry studies for TM_2X actually showing that it the case.[46,47]

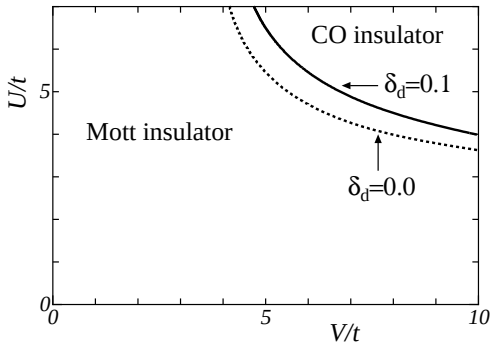

Fig. 8. Ground state phase diagram of the one-dimensional dimerized extended Hubbard model at quarter-filling on the plane of V/t and U/t, determined by the renormalization group equations for the bosonized phase Hamiltonian. The solid curve expresses the phase boundary between the charge ordered (CO) insulator and the dimer-type Mott insulator for $\delta_d = 0.1$,[80] while the dotted curve shows the boundary for $\delta_d = 0.0$ where the Mott insulating phase is replaced by the Tomonaga-Luttinger liquid[73] (see Fig. 4).

The interchain hopping t_{inter} generates warping of the Fermi surface in the non-interacting band structure. In $TMTSF_2X$ compounds, because of this effect, together with the weaker effect of Coulomb repulsion than in their TMTTF analogs, the strongly correlated insulators such as CO and dimer Mott insulators are not realized. Then the Fermi surface persists down to low temperatures. Such a dimensional crossover in half-filled models are theoretically discussed[82] while that in the quarter-filled CO systems remains to be investigated. This should be relevant to the pressure-induced melting of CO observed in DI-$DCNQI_2Ag$,[21] where the CO transition turns from a second order to a first order phase transtition by applying pressure, and a region with T^3-resistivity appears in the metallic state at the verge of the CO phase. In TM_2X, in contrast, the system becomes unstable due to the nesting of the Fermi surface toward a metal-insulator transition to an incommensurate spin-density-wave (SDW) ground state, which have also been studied intensively.[6,12,23]

Effects of the interchain Coulomb repulsion on the CO state have been discussed recently by Yoshioka *et al.*[83] by using the bosonization method described in the previous subsection. When one considers only one kind of uniform coupling in the interchain direction, it is expressed as,

$$\mathcal{H}_\perp = V_\perp \sum_{i,l} n_{i,l}n_{i,l+1}, \tag{7}$$

where l denotes the chain index. This may be applied

to the DCNQI compounds as the interchain coupling is uniform and isotropic while in TM_2X the network is more complicated as seen in Fig. 1 (we will consider them in § 2.6). In the "interchain MF" treatment,[84] the interchain part is treated within MF approximation as, $n_{i,l}n_{i,l+1} \to \langle n_{i,l}\rangle n_{i,l+1} + n_{i,l}\langle n_{i,l+1}\rangle - \langle n_{i,l}\rangle\langle n_{i,l+1}\rangle$, while quantum fluctuation within the 1D chains is incorporated. When $\langle n_i\rangle$ along the chains is written as $1/2+(-1)^i\delta$ where δ being the amplitude of CO, and an antiphase pattern of the Wigner crystal-type CO is assumed, the problem is reduced to an effective 1D model where δ is determined self-consistently. If δ is finite, an energy gap opens at $\pm 2k_{\rm F}$ and as a result the $4k_{\rm F}$-Umklapp scattering, $\tilde{\mathcal{H}}_{1/2}$, is generated, similarly to the case with finite dimerization discussed in § 2.3. However this Umklapp scattering is written with a cosine function of the phase variable but not with a sine function as in eq. (6), as follows,

$$\tilde{\mathcal{H}}_{1/2} = \frac{\tilde{g}_{1/2}}{2(\pi\alpha)^2}\int {\rm d}x \cos 2\theta_\rho, \tag{8}$$

where $\tilde{g}_{1/2}$ is proportinal to δ as long as $|\delta| \ll 1$. Therefore, different from the case with dimerization the generated non-linear term does not compete but cooperate with the $\cos 4\theta_\rho$ term when $g_{1/4} < 0$ in eq. (3). We note that such term, which acts as an alternating on-site potential upon the 1D chain, has been discussed from another context.[67] Thus, the interchain interaction stabilizes the antiphase CO, and the critical temperature $T_{\rm CO}$ becomes finite. Renormalization group study on this phase Hamiltonian[83] indicates that an infinitesimal value of $V_\perp$ gives rise to finite $T_{\rm CO}$ as long as $K_\rho < 1/2$ in the original 1D EHM model. This results in a sudden enlargement of the CO insulating region in the $U-V$ phase diagram once $V_\perp$ is considered, from the case of the 1D EHM where the phase boundary is determined by $K_\rho = 1/4$, as in Fig. 4.

2.5 Coupling to the lattice

1D electron systems are unstable when there exist couplings to the lattice degree of freedom. A well known case is the $2k_{\rm F}$ CDW (Peierls) instability, where electron gas becomes unstable at low temperatures toward a lattice distortion of period $2k_{\rm F}$ when the nesting condition of the Fermi surface is satisfied.[12] In the purely 1D case this condition is perfect so that any 1D electron system is susceptible to the Peierls-Frölich state. Another case is when the electrons are localized due to strong correlation and the spin degree of freedom is described by a 1D Heisenberg chain. There, the spin-lattice coupling makes the system unstable toward a spin-singlet formation accompanied with a lattice distortion, i.e., the spin-Peierls (SP) transition.[85,86] In fact, SP transition is frequently observed in many quasi-1D A_2B compounds, while its interplay with the charge sector such as the CO and the dimer Mott insulators is not obvious.

Let us first consider the so-called Peierls-type coupling to the lattice degree of freedom, treated as classical variables here neglecting quantum fluctuations, in addition to $\mathcal{H}_{\rm 1D}$ in eq. (2) with $\delta_{\rm d} = 0$. This allows modulations of the transfer integrals at the cost of the elastic energy, i.e., $t \to t(1+u_{i,i+1}) + Ku_{i,i+1}^2/2$, where $u_{i,i+1}$ is the dimensionless modulation of the lattice, controlled by the actual movement of the molecules i and $i+1$. K is the renormalized lattice constant, which is taken to be uniform here but in general, as in the discussion in § 2.1 on V_{ij}, can be modulated; for example in the 1D model of TM_2X it would be dimerized as K_{a1} and K_{a2} (see Fig. 1). Hereafter we write $u_{i,i+1} = u_i$ for simplicity. The "softness" of the lattice is indicated by $1/K$; at $K \to \infty$ the system is in the "hard" limit so that the lattice does not move and then the model reduces to the purely electronic model, $\mathcal{H}_{\rm 1D}$.

One serious effect of this coupling is that it can generate the dimer Mott insulating state even without intrinsic dimerization ($\delta_{\rm d} = 0$). This is understood in the $U/t = \infty$ limit discussed by Bernasconi *et al.*[66] Extending the discussion in § 2.2, the charge degree of freedom described by the half-filled interacting SF or equivalently the $S = 1/2$ XXZ model is now coupled to the lattice. In the latter model the Peierls coupling appears in the XY term, J_{xy}; for $J_{xy} = 2t \geq J_z = V$, infinitesimal spin lattice coupling $1/K$ can drive the ground state toward SP lattice dimerization.[85] This is actually the dimer Mott insulator when one transforms back to the original electron model. This state competes with the CO state at large V/t, and the transition point $V_{\rm cr}/t$ increases with increasing $1/K$.[87,88]

When U/t is finite, the spin degree of freedom (in the original electronic model) becomes active. The model have been treated by different numerical techniques[62,89–91] as well as by the bosonization method.[91,92] As discussed in the previous subsections, the latter treatment can clarify the physical origin of each state which is realized. A phase Hamiltonian is derived following the treatment in § 2.3, where nonlinear terms additional to $\mathcal{H}_\rho$ in eq. (3) and $\mathcal{H}_\sigma$ are generated in the presence of the lattice dimerization $u_{\rm d}$ and tetramization $u_{\rm t}$, with a cost of lattice elastic energy $\mathcal{H}_{\rm el}$. These can be expressed as

$$\mathcal{H}_{\rm d} = -\frac{g_{1/2}u_{\rm d}}{2(\pi\alpha)^2}\int {\rm d}x \sin 2\theta_\rho, \tag{9}$$

$$\mathcal{H}_{\rm t} = -\frac{g_{\rm t}u_{\rm t}}{2(\pi\alpha)^2}\int {\rm d}x \sin(\theta_\rho - \chi_{\rm t})\cos\theta_\sigma, \tag{10}$$

when the lattice distortion is parametrized as $u_i = u_{\rm d}\cos(\pi x_i/a) + u_{\rm t}\cos(\pi x_i/2a + \chi_{\rm t})$ where χ_t is a phase factor. The term in eq. (9) is the $4k_{\rm F}$-Umplapp term having the form identical to eq. (6) except the presence of $u_{\rm d}$. Therefore provided $u_{\rm d} \neq 0$ it can actually produce the dimer Mott insulator. On the other hand, in eq. (10), $g_{\rm t} \propto t$ couples the two phase variables for charge (θ_ρ) and spin (θ_σ). In the weakly correlated regime this term shows the instability of the system toward the $2k_{\rm F}$ CDW state.[79]

In the strongly correlated regime, on the other hand, the competition between the CO insulator ($\theta_\rho = 0$ or $\pi/2$) and the dimer Mott insulator ($\theta_\rho = \pi/4$) arises due to the $8k_{\rm F}$-Umklapp term in $\mathcal{H}_\rho$ and the $4k_{\rm F}$-Umklapp term eq. (9), respectively. This is similar to the case in § 2.3 for $\mathcal{H}_{\rm 1D}$ in eq. (2) with $\delta_{\rm d} \neq 0$, although here, $u_{\rm d}$, and consequently the presence of the $4k_{\rm F}$-Umklapp

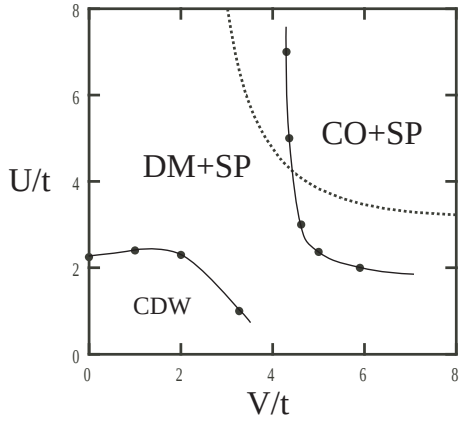

Fig. 9. Ground state phase diagram of the one-dimensional extended Peierls-Hubbard model at quarter-filling calculated by the density matrix renormalization group method,[91] on the plane of U/t and V/t for fixed values of $1/K = 0$ (dotted line, equivalent to Fig. 4) and $1/K = 1$ (filled line). CO-SP, DM-SP, and CDW phases denote the coexistent state of charge order and spin-Peierls lattice tetramization, that of dimer Mott insulator and spin-Peierls lattice tetramization, and the weak coupling Peierls-Frölich state. [After ref. 91.]

term itself, should be determined self-consistently. The spin degree of freedom in these two states is derived to be described by the same phase Hamiltonian $\mathcal{H}'_\sigma = \mathcal{H}_\sigma - g_t u_t \int \mathrm{d}x \cos\theta_\sigma + \mathcal{H}_{\rm el}$, which is identical to that of the SP model.[86] Therefore the two insulating states above are both unstable toward the non-magnetic SP state with lattice tetramization, $u_t \neq 0$, resulting in coexistent states.

These symmetry broken states are in fact reproduced in the numerical calculations. Let us show a ground state phase diagram by Kuwabara *et al.*[91] determined by the numerical DMRG method in Fig. 9. The spatial modulation of the lattice distortion at each site is determined self-consistently and system sizes up to $L = 36$ are needed to diminish the finite-size effect. One can see that all the states predicted in the phase Hamiltonian appear in different regions of parameters $(U/t, V/t)$. For the actual pattern of charge density and lattice distortion in each state, see ref. 91.

There is another type of coupling to the lattice degree of freedom from the Peierls coupling above: the Holstein coupling, which describes modulation of the one-particle on-site energy at the cost of elastic energy. The origin of this coupling can be the electron-molecular vibration (e-mv) coupling frequently discussed in molecular systems.[93] This coupling is usually not large such that the nature of phenomena due to strong correlation discussed in this review is qualitatively modified. However, recently, exceptionally large deformation of molecules themselves coupled to charge disproportionation in $(EDO\text{-}TTF)_2PF_6$ is observed,[94] suggesting large e-mv coupling in this material.[95] Another source for the Holstein-type coupling recently considered affecting the CO state is the influece of the X^- unit implied by experiments in TM_2X.[22,37] The ferroelectricity observed below the CO temperature is interpreted as the combination of CO state in the dimerized stack of TM molecules (see Fig. 6) and the $\boldsymbol{q} = 0$ motion of the anions, producing large electrical polarization.

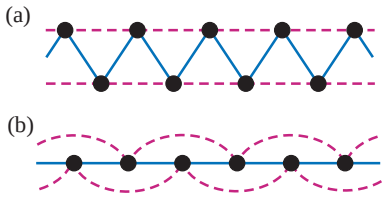

Fig. 10. (Color online) (a) Zigzag ladder and (b) one-dimensional chain with next nearest neighbor interactions. These two are equivalent with each other as seen in the figure.

Numerical ED calculations for small cluster sizes up to about $L = 16$ sites including this Holstein coupling as well as the Peierls coupling suggests that the former type works toward stabilization of the CO state in general.[62,96] We note that since the lattice is 3D in nature, these couplings would result in finite temperature phase transitions,[92] which are not fully investigated yet. Furthermore, the inclusion of intrinsic dimerization $\delta_{\rm d}$ in the model might modulate the results, such as a further stabilization of the dimer Mott insulating state.[92,96] Still, systematic works which would provide unified pictures of the quasi-1D electron-lattice coupled quarter-filled systems, together with the interchain coupling discussed in § 2.4, are to be done.[97]

2.6 Geometrical frustration

As introduced in § 2.4, the interchain Coulomb interaction $V_\perp$ added to the 1D EHM stabilizes the 2D or the 3D CO state with an anti-phase pattern between chains. However, in the actual molecular materials the manner of coupling between chains is frequently more anisotropic. For example, in TM_2X, as shown in Fig. 1, three kinds of interchain bonds are formed in a zigzag way. Then the interchain Coulomb repulsion V_b favors the CO pattern along the b-direction to be anti-phase between chains, while V_{p1} and V_{p2} favor the in-phase pattern. (The observed ferroelectricity in ref. 37 points to the latter.) Since these Coulomb energies are expected to have similar values,[46,47] the two CO patterns compete with each other. This is an example of geometrical frustration.

Effects of the geometrical frustration are intensively studied in localized spin systems[98] defined on lattice structures with odd number of sites when rounding along the bonds of a cell, e.g., triangular forms as in the above example of TM_2X. It is known to drive the system toward destabilization of the classical antiferromagnetic state and sometimes even result in a total destruction of it, namely, in a spin disordered state. The analogy between the classical picture of CO and the spin systems noted in § 2.2 naturally leads us to the problem of geometrical frustration in CO systems, where the CO may be destabilized as well. This was first considered by Anderson[52] in the context of the "classical" 3D CO system, magnetite Fe_3O_4, described as an Ising model on the phyloclore lattice which is a typical frustrated lattice structure.

Treating the zigzag coupling in the 2D model for TM_2X with full anisotropy is a problem yet to be solved. A similar situation will be discussed in § 3.3, related to the CO in quasi-2D θ-ET_2X. Instead, here we

consider a more simple system but having many common aspects: a double-chain system with zigzag couplings between them, i.e., a zigzag ladder, shown in Fig. 10. As seen in Fig. 10, it is equivalent to a 1D model with next-nearest-neighbor interactions. Then the EHM on this chain structure can be written as $\mathcal{H}_{1D}$ in eq. (2) with $\delta_d = 0$ added by next-nearest terms, $t_2 \sum_{i\sigma}(c^\dagger_{i\sigma} c_{i+2\sigma} + \text{h.c.}) + V_2 \sum_i n_i n_{i+2}$. In the following we write the nearest neighbor terms as t_1 and V_1.

This model at quarter-filling has been studied as an effective model for two different material systems. One is for $TMTSF_2X$, with $t_2 = 0$, extending the range of Coulomb interaction terms from the previous works.[74,99] Another is for the Cu-O subunit of a transition metal oxide $PrBa_2Cu_4O_8$, where the effective model for the Cu sites has a zigzag ladder structure with $t_1 \ll t_2$, and $V_1 \simeq \sqrt{2}V_2$ suggested by the Cu-Cu distances.[100,101] For $t_1 = 0$ or $t_2 = 0$, the model at $U = \infty$ is exactly mapped onto XXZ models when one follows the mapping of Ovchinnikov explained in § 2.2, therefore the analogy between the frustrated localized spin system and the CO system is straightforward here again.

For the $t_2 = 0$ case, Emery and Noguera[102] actually studied the 1D XXZ model with next nearest J_z term, while Yoshioka *et al.*[74] studied the finite-U case by the method described in § 2.3. In these studies the interaction terms are treated perpurbatively from the weak-coupling regime. They have discussed the competition between two different CO patterns favored respectively by V_1 and V_2. The one favored by V_2 having wave vector $2k_F$ (k_F defined for $t_2 = 0$) shows $2k_F$ SDW correlation developped. The co-existent state of $2k_F$ SDW and $2k_F$ CDW was first proposed based on the MF approximation,[99] to discuss such state observed in $TMTSF_2X$.[50] We note that this "$2k_F$" CDW is different from the Peierls-Frölich state due to electron-lattice coupling, but it is originated from the strong correlation, V_2, i.e., it is indeed a CO state. A possible insulating bond ordered wave phase is also found in the above weak-coupling approaches, in the competing region.

Numerical studies on such models on the zigzag ladder have found a different aspect at large V_{ij}'s where the weak coupling approaches above may break down: a wide region of the metallic TLL phase between the two CO phases.[100] A phase diagram by the numerical DMRG method is shown in Fig. 11,[103] where TLL phase is widely realized in the $V_1 \simeq 2V_2$ region, with K_ρ close to 1/4 suggesting the closeness to CO. This is a consequence of the geometrical frustration, and in such metallic phase with both V_1 and V_2 having large values, the existence of large fluctuations of both CO states is expected.[104]

Recently, it is pointed out that the CO state in DI-DCNQI$_2$Ag is affected by similar geometrical frustration. This is due to a peculiar situation where the interchain configuration along each plaquette in the a-b plane (see Fig. 1) has a spiral symmetry which is not compatible with the twofold periodicity generated by CO.[105] Such frustration due to the spiral symmetry is also found to exist in the process of the metal-insulator transition in DMe-DCNQI$_2$Cu,[106] where the π-electron couples to the Cu d-electron producing a three-fold periodic structure[107] again not compatible with the spiral symmetry, which is beyond the scope of this review.

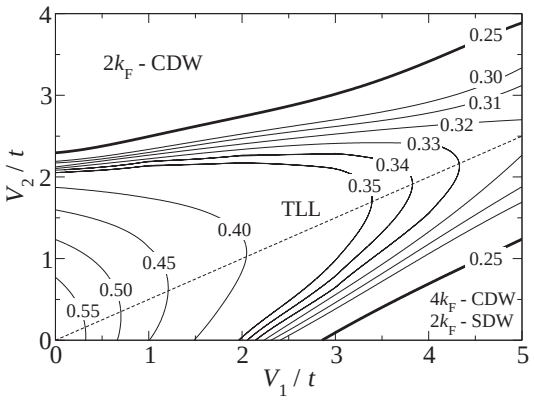

Fig. 11. Ground state phase diagram of the extended Hubbard model at quarter-filling on the zigzag ladder, determined by the density matrix renormalization method.[103] U/t_1 is fixed at 10 while t_2 is set to 0. Sandwitched by the two insulating CO phases with different charge patterns, the Tomonaga-Luttinger liquid (TLL) metallic phase is extended toward the frustrated line $V_1 = 2V_2$. The contour lines indicate the TLL parameter K_ρ. [Reprinted figure with permission from S. Ejima *et al.*, Phys. Rev. B **72** (2005) 033101. Copyright (2005) by the American Physical Society.]

3. Quasi-Two-Dimensional Systems

Many theoretical works on CO states in 2D models near half-filling have been performed, such as in the Hubbard model and in the t-J model on the square lattice, mainly devoted to the high-T_c SC cuprates and related transition metal oxides.[108] However, studies on the quarter-filled case are mostly triggered by the recent experimental findings of CO in quasi-2D molecular conductors. To the authors' knowledge, only a few have been done beforehand. Ohta *et al.*[109] studied the 2D EHM on the square lattice for different fillings including one quarter, in fact motivated by the cuprates, while a more specific case was studied[110] to explain the CO transition in NaV_2O_5 (see § 4).

Since CO has been found in many quasi-2D A_2B systems such as in ET_2X, theoretical works have been performed on the 2D EHM adopting the full anisotropy (or a part of it) of the materials. On the other hand, the quarter-filled EHM on the square lattice has been studied as well from a rather general viewpoint. Such 2D models are difficult to analyze theoretically in a controlled way, and intensive efforts are now in progress. We will review the present status in this section.

3.1 Charge ordering in quasi-two-dimensional systems

Direct observation of the CO transition in quasi-2D A_2B compounds was first in θ-$ET_2RbZn(SCN)_4$,[4,111] and next in α-ET_2I_3,[112] both found in ^{13}C-NMR experiments. Now many quasi-2D A_2B materials, including non-ET based compounds, are recognized to show CO.[25] Their crystal structures are composed of alternating layers of A molecules and B units, and quasi-2D electronic states are realized; t_{ij} along the interlayer direction are small due to the insulating B layers. These materials

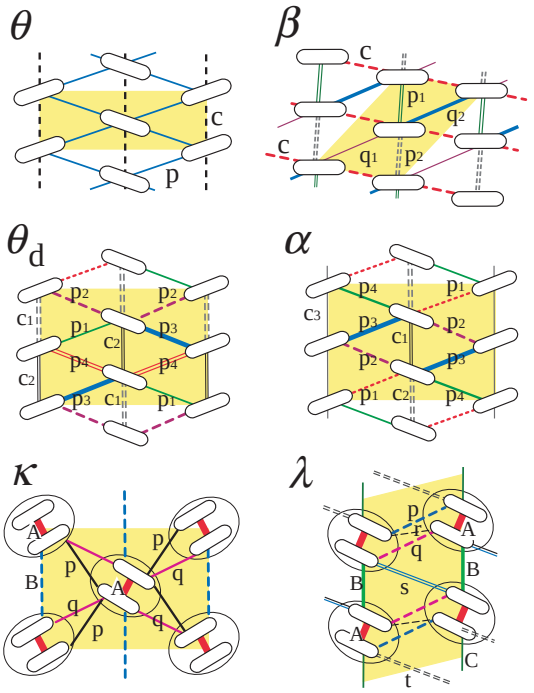

Fig. 12. (Color online) Schematic representation of the 2D layers in different polytypes of quasi-2D A_2B materials. The indices are not only for t_{ij} but also for different values of V_{ij}, although the degree of anisotropy can be different (see text). In the κ-type and the λ-type structures the thick A bonds are those with the transfer integral t_A considerably larger than the others, i.e., dimers. [By courtesy of C. Hotta.]

have a variety in their 2D arrangements of A molecules, sometimes even for the same chemical formula, i.e., polytypes, classified by greek characters, α, β, κ, θ, λ, and so on.[45] Some representative examples are shown in Fig. 12, for which the actual values of transfer integrals calculated by the extended Hückel method we refer to, e.g. refs. 8 and 45. Because of such anisotropy in the lattice structures, the EHM we should treat, $\mathcal{H}_{\rm EHM}$ in eq. (1), would be complicated. As was mentioned in § 1, we emphasize that such diversity of lattice structures here is one of the important characteristics producing the rich variety of properties in molecular conductors. CO is in fact very much affected by such geometry of the lattice as we will see in the following subsections.

A theoretical approach to handle this diversity was pursued by Kino and Fukuyama,[17] who considered Hubbard models ($V_{ij}=0$) for ET_2X, taking into account the full anisotropy in t_{ij} for each polytype, and applied MF approximation to the on-site Coulomb interaction term U. By this they have provided a way to search for relations between the crystal structure and electronic properties, and also for generic understandings even among different polytypes.[113] Since the polytypes show a variety, different ways of such systematic views have been discussed by different authors since then.[8,45,114] One way is to consider an anisotropic triangular lattice,[19,115] refined by Hotta[114] as follows.

In Fig. 12, one can see that θ, α, and β-type structures have the triangular lattice as basis, "colored" with anisotropy. Since the charge transfer is realized as $[ET_2]^+X^-$, the one-particle HOMO bands as a whole are quarter-filled in terms of holes. Effective models for the materials with these symmetries would be the quarter-filled EHM on an anisotropic triangular lattice, with V_{ij} having the same anisotropy as t_{ij}. For example, for the θ-type structure with highest symmetry among the polytypes,

$$\mathcal{H}_\theta = -t_p \sum_{\langle ij\rangle_p,\sigma} (c^\dagger_{i\sigma}c_{j\sigma}+h.c.) - t_c \sum_{\langle ij\rangle_c,\sigma} (c^\dagger_{i\sigma}c_{j\sigma}+h.c.) + U\sum_i n_{i\uparrow}n_{i\downarrow} + V_p \sum_{\langle ij\rangle_p} n_i n_j + V_c \sum_{\langle ij\rangle_c} n_i n_j, \quad (11)$$

where $\langle ij\rangle_p$ and $\langle ij\rangle_c$ denotes the site pairs i and j along the p bonds and the c bonds, respectively. In contrast, κ and λ-type stuctures consist of dimers, i.e., pairs of molecules connected by t_{ij} considerably larger than the others, indicated as the A bonds in Fig. 12; if one considers the dimers as units, these structures are topologically equivalent to θ and β-type structures, respectively. Half-filled models on the anisotropic triangular lattice can be effective models for such systems with large dimerization. Then the on-dimer Coulomb repulsion $U_{\rm dimer}$ can lead the system toward the dimer Mott insulator (see refs. 8, 17-20).

The CO states are stabilized in the former quarter-filled models. In Kino and Fukuyama's work on the Hubbard model for α-ET_2I_3,[116] an insulating state accompanied with charge disproportionation between stacks (the vertical stripe type CO pattern; see § 3.3) is found. However, the charge pattern there is not consistent with later experiments. Moreover in a MF study on the Hubbard model for the other CO material θ-$ET_2RbZn(SCN)_4$, CO state is not even stabilized.[117] Following these works, V_{ij} added to the Hubbard model retaining the full anisotropy in t_{ij}, i.e., the EHM for ET_2X on the anisotropic triangular lattice, has been introduced by Seo,[118] who discussed the CO states there based on the MF approximation. As in the quasi-1D systems discussed in § 2, the intersite Coulomb interaction is also crucial for CO in the quasi-2D materials.

The values of V_{ij} are in fact estimated to be appreciable compared to U. As in the quasi-1D compounds in § 2, U is believed to be of the order of 1 eV in the ET compounds as well, while, again, the actual values for V_{ij}/U estimated as $0.2 \sim 0.7$[119–121] are too ambiguous for quantitative arguments. Typical values for $|t_{ij}|$ in the ET materials estimated by the extended Hückel method range around $0.1 \sim 0.25$ eV.[8,45] Therefore these materials are indeed strongly correlated systems. We note again that the degree of anisotropy in t_{ij} and that in V_{ij} does not correspond in a one-to-one manner. For example in many members of θ-ET_2X described by eq. (11), $|t_c|$ is much smaller than $|t_p|$,[24] despite of their close intermolecular distance resulting in $V_c \simeq V_p$.[121]

The anisotropic triangular lattice is somewhat complicated and therefore it is not only tough to handle it theoretically but also sometimes difficult to extract explicit key parameters for the physics therein. One natural way of thinking, as was pointed out by McKenzie *et al.*,[122] is to study the quarter-filled EHM on the square lattice, which is much simpler but would still show essential features of the CO transition in 2D, and even of the

expected SC state[123] (§ 3.4). In this model, there is one kind of transfer integral t and also inter-site Coulomb repulsion V, along nearest-neighbor sites both in x and y directions. Such studies on the square lattice can shed light on the properties of the anisotropic triangular lattice EHM, as the former is one of the limiting cases of the latter. For example, in the θ-type structure if we set $t_c = 0$, $V_c = 0$ and $t = t_p$, $V = V_p$, $\mathcal{H}_\theta$ in eq. (11) becomes equivalent to the square lattice EHM. Neglecting t_c is in fact a good approximation for θ-ET_2X whereas V_c cannot be neglected, as mentioned above, while this square lattice case might be applied to some β''-type compounds.[123] Note that electron-hole symmetry holds in the square lattice EHM while t_c breaks it, so relative signs between t_{ij} become distinct. We will explain studies on the square lattice EHM first (§ 3.2) and then the anisotropic triangular lattice case next (§ 3.3), although the research has been developped more or less in a parallel way.

3.2 Extended Hubbard model on square lattice

The existence of a checkerboard type CO with wave vector $\boldsymbol{q}$=$(\pi/a, \pi/a)$ on the quarter-filled square lattice EHM, as shown in Fig. 13, has been first demonstrated by Ohta *et al.*,[109] for $U = 8t$ and $V = 3t$. It is based on calculations of the equal-time charge correlation function $C(\boldsymbol{q}) = L^{-1}\sum_{ij}\langle n_i n_j\rangle e^{i\boldsymbol{q}\cdot\boldsymbol{R}_{ij}}$, where L is the total number of sites in the square shaped clusters and $\boldsymbol{R}_{ij}$ is the vector connecting site i and j, by use of the Lanczos ED technique with cluster sizes up to $L = 16$. This pattern can be understood naturally as the extention of the 1D case (Fig. 2(a)) from the idea of "Wigner crystal on lattice".

They have also derived an effective spin model in such CO state by the fourth order perturbative expansion from strong coupling, $t \ll (U, V)$. It is an antiferromagnetic Heisenberg model on the square lattice, rotated 45 degrees from the original lattice (see Fig. 13), with a nearest neighbor exchange coupling,

$$J = \frac{4t^4}{9V^2}\left(\frac{4}{U} + \frac{1}{V} + \frac{4}{U+4V}\right). \qquad (12)$$

Note that even at $U/t = \infty$, novel ring exchange processes break the zeroth order spin degeneracy resulting in a finite $J = 4t^4/9V^3$.[122] Since the next-nearest-neighbor coupling J' is estimated to be much smaller, an antiferromagnetic spin order as shown in Fig. 13 is expected at the ground state since the square lattice Heisenberg model shows Néel order.[124]

A systematic numerical Lanczos ED study was demonstrated by Calandra *et al.*,[125] for cluster sizes up to $L = 20$. In this case, a powerful method to determine from small systems whether the bulk system is metallic or insulating is to evaluate the Drude weight D.[126–128] It is given by

$$\frac{D}{2\pi e^2} = -\frac{\langle 0|K|0\rangle}{4L} - \frac{1}{L}\sum_{n\neq 0}\frac{|\langle n|j_x|0\rangle|^2}{E_n - E_0}, \qquad (13)$$

where E_0 and E_n denote the ground state ($|0\rangle$) and excited state ($|n\rangle$) energies of the system, respectively.[59] K is the kinetic energy operator and j_x is the current operator in the x direction at zero wavevector ($\boldsymbol{q} = 0$). The occurrence of an insulating phase is marked by the exponential vanishing of D with the linear size of the system $L_x = \sqrt{L}$.[126,128] In Fig. 14 the results are shown, where D is plotted as a function of V/t for different U/t. As V/t is increased, D decreases until it eventually vanishes. For $U/t = 10$ the critical value for the metal-insulator transition is estimated as $V_{\rm cr}^{\rm MI}/t \simeq 2.2$. We should note that this might not be conclusive as an accurate value as the finite size scaling shown in the inset of Fig. 14 is only for the three clusters L=8, 16, and 20, due to computorwise limit. Nevertheless, for $V > V_{\rm cr}^{\rm MI}$, D displays an exponential dependence with $1/L_x$ as expected for an insulator,[126,128] while for $V < V_{\rm cr}^{\rm MI}$, in contrast, it weakly depends on $1/L_x$ extrapolated to a finite value in the thermodynamic limit, consistent with a metallic state. On the other hand, the occurrence of CO has been investigated by computing $C(\boldsymbol{q})$ systematically. The extrapolation suggests $V_{\rm cr}^{\rm CO}/t \simeq 1.6$, where $C(\pi/a, \pi/a)$ starts to show a peak as V is increased, which possibly overestimate its value due to finite size effects. When U decreases the critical value $V_{\rm cr}^{\rm CO}$ increases, similarly as in the 1D case (see Fig. 4).

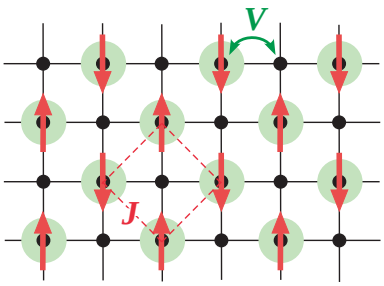

Fig. 13. (Color online) Checkerboard charge ordered insulating ground state of the square lattice extended Hubbard model at quarter filling in large U/t and V/t. An antiferromagnetic interaction J occurs between spins along the diagonals shown in the figure.

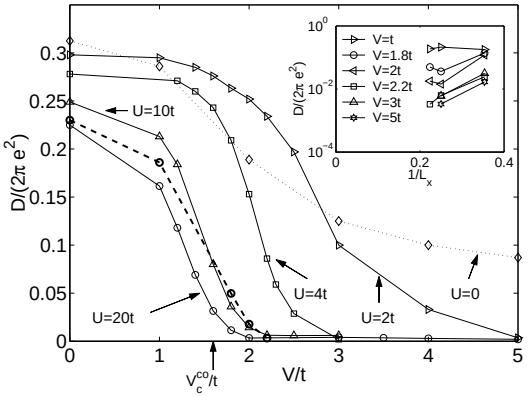

Fig. 14. The Drude weight, D, for the quarter-filled square lattice extended Hubbard model as a function of V/t, for $L = 16$ and various values of U/t (continous and dotted lines), and for $L = 20$ and $U = 10t$ (dashed line).[125] The arrow in the horizontal axis marks the onset of checkerboard charge ordering for $U = 10t$. The inset shows the finite-size scaling of D as a function of $1/L_x$ for different values of V/t with $U = 10t$. The metal-insulator transition occurs at $V_{\rm cr}^{\rm MI} \simeq 2.2t$. [Reprinted figure with permission from M. Calandra *et al.*, Phys. Rev. B **66** (2002) 195102. Copyright (2002) by the American Physical Society.]

Since the estimates above provide $V_{\rm cr}^{\rm MI} > V_{\rm cr}^{\rm CO}$, a possible CO metallic phase, not found in the 1D EHM, is suggested. In fact, a recent variational Monte-Carlo calculation[129] (see next subsection) have confirmed its existence, with a CO metallic phase realized between the uniform metallic and the CO insulating phases, i.e., at $V_{\rm cr}^{\rm CO} < V < V_{\rm cr}^{\rm MI}$. We note that another work using projector correlated method[130] shows that such feature is also seen at finite temperatures. This is in clear contrast with the purely 1D EHM discussed in § 2, where the quantum fluctuation destroys the finite-T CO phase transition. More theoretical efforts are needed, to explore the overall phase diagram for this model, in the (U, V, T) parameter space, for the critical values of CO, metal-insulator, and antiferromagnetic phase transitions.

Although the analysis above is restricted to numerics, the $U/t = \infty$ limit has been investigated analytically by McKenzie *et al.*[122] In this limit the square lattice EHM reads after projecting out the doubly occupied sites as

$$\mathcal{H}_{tV} = -t \sum_{\langle ij\rangle\sigma} \mathcal{P}\left(c_{i\sigma}^\dagger c_{j\sigma} + h.c.\right)\mathcal{P} + V\sum_{\langle ij\rangle} n_i n_j, \quad (14)$$

where $\mathcal{P}$ projects out the doubly occupied configurations due to their prohibition at $U/t = \infty$. We refer to this model as the t-V model; this is the generalization of the $U/t = \infty$ limit of the 1D case discussed in § 2.2, whereas the charge and spin degree of freedoms cannot be decoupled in 2D.

They have introduced an SU(N) generalization of this model in which the spin index runs from 1 to N, and carried out a slave boson theory, which have been applied to various models for strongly correlated electron systems by different authors.[131] The electron creation operator is replaced by $c_{i\sigma}^\dagger = f_{i\sigma}^\dagger b_i$, where the spinless charged boson operator b_i is introduced to keep track of the empty sites, and $f_{i\sigma}^\dagger$ is a fermion operator carrying spin. In order to preserve the anticommutation relation for the electrons the new operators must satisfy the local constraint $f_{i\sigma}^\dagger f_{i\sigma} + b_i^\dagger b_i = N/2$. Hereafter, whenever a repeated σ index appears a sum from 1 to N is assumed. Note that the original EHM has $N = 2$.

In the coherent state path integral formulation[132] the Lagrangian at imaginary time τ is given by

$$\begin{aligned} L(\tau) = &\sum_i \left(f_{i\sigma}^\dagger(\partial_\tau - \mu) f_{i\sigma} + b_i^\dagger \partial_\tau b_i\right) \\ &-\frac{t}{N}\sum_{\langle ij\rangle}(f_{i\sigma}^\dagger f_{j\sigma} b_j^\dagger b_i + h.c.) + \frac{V}{N}\sum_{\langle ij\rangle} f_{i\sigma}^\dagger f_{i\sigma} f_{j\sigma'}^\dagger f_{j\sigma'} \\ &+ \sum_i i\lambda_i (f_{i\sigma}^\dagger f_{i\sigma} + b_i^\dagger b_i - N/2), \end{aligned} \quad (15)$$

where μ is the chemical potential and λ_i is a static Lagrange multiplier enforcing the local constraint above. We have used the fact that $c_{i\sigma}^\dagger c_{i\sigma} = f_{i\sigma}^\dagger f_{i\sigma}$.

Following Kotiar and Liu's work on the square lattice Hubbard model,[132] it is convenient to choose the radial gauge to avoid possible infrared divergences where the boson amplitude becomes a real number, $r_i = |b_i|$, and λ_i becomes a dynamical bosonic field: $\lambda_i(\tau)$. By using the relation $f_{i\sigma}^\dagger f_{i\sigma} = N/2 - b_i^\dagger b_i$ to replace one pair of fermion operators in the V term and integrating out the other fermionic degree of freedoms, we are left with an effective Lagrangian which is quadratic in the boson fields.

The MF solution of the effective bosonic model is obtained by assuming that the boson fields are spatially homogeneous and time independent: $r_i(\tau) = b$ and $i\lambda_i(\tau) = \lambda$. This treatment is exact in the $N \to \infty$ limit, therefore is a base for the expansion in powers of $1/N$.[131,132] The resulting MF free energy is

$$F^{\rm MF}(b, \lambda) = -\frac{N}{\beta}\sum_{\boldsymbol{k},\omega_n} \ln(\epsilon_{\boldsymbol{k}} - i\omega_n) + \lambda(b^2 - \frac{N}{2}), \quad (16)$$

where $\beta = 1/(k_{\rm B}T)$ and ω_n is the fermion Matsubara frequency. The MF eigenenergy is given by $\epsilon_{\boldsymbol{k}} = -2tb^2(\cos k_x + \cos k_y)/N + \lambda - \mu + 4Vn/N$. Minimization of $F^{\rm MF}$ with respect to b and λ leads to $b^2 = N/2 - n$, $\lambda = 2t\sum_{\boldsymbol{k}} f(\epsilon_{\boldsymbol{k}})(\cos k_x + \cos k_y + 4V)$. and μ is adjusted to give the correct electron filling. This form, eq. (16), indicates that the MF solution for the large-N generalized t-V model describes just a renormalized Fermi liquid, analogous to the case of the Hubbard model.[132] In the case of quarter-filling and $N = 2$ (which is somewhat artificial as one implicitly consider N to be large), the bandwidth is reduced to half its bare value as $b^2 = 1/2$ and the band is shifted from its bare position by λ. Namely, the mass is enhanced as twice the bare value, i.e., $m^*/m = 1/b^2 = 2$. The overall effect of the nearest-neighbour Coulomb interaction, V, reduces to a constant shift in the chemical potential.

The leading $1/N$ corrections modify the MF solution so that when V/t is increased the Fermi liquid phase results in an instability toward the checkerboard type CO state. This is seen when writing the boson fields in terms of the static MF solution (b, λ) and the dynamic fluctuating parts: $r_i(\tau) = b + b\delta r_i(\tau)$, and $i\lambda_i(\tau) = \lambda + i\delta\lambda_i(\tau)$. The resulting effective action, to the second order in the boson fields, is $S = F^{\rm MF} + S^{(2)}$, where the second term due to the fluctuations in the boson fields is written in the form as

$$\begin{aligned} S^{(2)} = \frac{1}{2\beta}\sum_{\boldsymbol{q},\nu_n} &\left[\ \delta r(-\boldsymbol{q}, -\nu_n) \quad \delta\lambda(-\boldsymbol{q}, -\nu_n)\ \right] \times \\ &\begin{pmatrix} \Gamma_{rr} & \Gamma_{r\lambda} \\ \Gamma_{\lambda r} & \Gamma_{\lambda\lambda} \end{pmatrix} \begin{pmatrix} \delta r(\boldsymbol{q}, \nu_n) \\ \delta\lambda(\boldsymbol{q}, \nu_n) \end{pmatrix}, \end{aligned} \quad (17)$$

where ν_n is the boson Matsubara frequency; for the explicit form of the elements in $\hat{\Gamma}(\boldsymbol{q}, \nu_n)$ see ref. 122. We note that $\Gamma_{\lambda\lambda}$ is the Lindhard function describing density-density fluctuations in the renormalized band. The propagators of the boson fields $\hat{D}(\boldsymbol{q}, \nu_n) = \hat{\Gamma}^{-1}(\boldsymbol{q}, \nu_n)$ are of the order $O(1/N)$, as they should. The condition for an instability of the Fermi liquid phase is when the quadratic form (17) becomes negative at some $\boldsymbol{q}$ for $\nu = 0$, so that fluctuations in the charge density will decrease the free energy. This is determined by $\det\hat{\Gamma} < 0$ at $\boldsymbol{q} = (\pi/a, \pi/a)$ for quarter filling, which provides $(V/t)_{\rm cr} = 0.69$ for the critical value from the Fermi liquid to the CO state for this large-N t-V model. We note that the inclusion of diagonal hopping t' (equivalent to t_c in eq. (11)) is easily incorporated in this scheme, which does not modify the results qualitatively.[122]

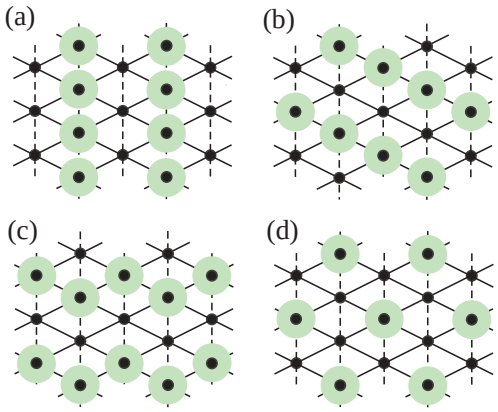

Fig. 15. (Color online) Charge ordered states in the quarter-filled extended Hubbard models on anisotropic triangular lattices: (a) vertical, (b) diagonal, and (c) horizontal stripe type states, and (d) the threefold state. Sites with/without colored circle represent the charge rich/poor sites. The solid and dotted bonds represent the "p" ($p1 \sim p4$) and "c" ($c1 \sim c3$) bonds in the θ(or $\theta_{\rm d}$)-type and the α-type structures in Fig. 12.

3.3 *Extended Hubbard model on anisotropic triangular lattice*

As we have seen in the previous subsection, the intersite Coulomb repulsion can drive the system toward CO in 2D systems as well. In the strongly correlated regime, the spins are described by an effective 2D Heisenberg model with spins located on the charge rich sites. Such aspects are common with the 1D cases discussed in § 2, where CO results in magnetic properties of 1D Heisenberg chains. These knowledges are very useful in treating the more anisotropic cases introduced in § 3.1, with full anisotropy taken into account. There, calculations beyond MF are still in progress, but if we deduce from the MF results together with the picture above, qualitative understandings of the experiments can be obtained[18] as follows.

MF calculations on the anisotropic triangular lattice EHM were first performed by Seo[118] for different materials with θ and α-type structures. The U and the V_{ij} terms are treated within the standard MF treatment as $n_{i\sigma}n_{j\sigma'} \to n_{i\sigma}\langle n_{j\sigma'}\rangle + \langle n_{i\sigma}\rangle n_{j\sigma'} - \langle n_{i\sigma}\rangle\langle n_{j\sigma'}\rangle$, by allowing large unit cell sizes to consider various CO states with several possible spin orders for each of them. In fact many self-consistent MF solutions are obtained and their ground state energies are compared. It is found that CO states with lowest energy show a variety as shown in Fig. 15 depending on the parameters, which is in contrast to the square lattice case where the checkerboard pattern is stable. Mainly the "stripe" type CO states are discussed in ref. 118, shown in Fig. 15(a) $\sim$ (c), where the carrier densities on the charge rich and the charge poor sites are (in some cases approximately) $1/2+\delta$ and $1/2-\delta$, respectively. These can be considered as extensions of the Wigner crystal-type CO, which can lead to insulators in the strongly correlated regime. In general, the vertical stripe type pattern is favored by the Coulomb repulsion along the solid bonds in Fig. 15, while that along the dotted bonds stabilizes the diagonal and horizontal patterns.

Let us start with the MF results for the θ-type structure, eq. (11), which has the highest symmetry among the polytypes. As noted in § 3.1, nearly isotropic $V_c \simeq V_p$ is expected,[121] which gives rise to close competition between the different CO patterns. MF calculations[118] for eq. (11) at $T = 0$ considering the stripe type CO patterns as in Fig. 15(a) $\sim$ (c), have been performed for $t_p = -0.1$ eV, $t_c = 0.01$ eV, taken from typical extended Hückel parameters for θ-$ET_2MM'(SCN)_4$ (M: Rb, Cs, Tl, etc., and M': Zn, Co, etc.),[24] and $U = 0.7$ eV, while varying V_p and V_c near 0.3 eV. The results show that either vertical or diagonal stripe type CO solution is stabilized for $V_c \lesssim V_p$ and $V_c \gtrsim V_p$, respectively, whereas the horizontal pattern has rather higher MF energies. In the actual θ-type compounds which sustain this structure down to low temperatures, either vertical[133] or diagonal[134] pattern of CO is indicated by optical measurements, consistent with the MF results. We note that the vertical stripe CO state here is equivalent to the checkerboard pattern in the $t_c = 0$ and $V_c = 0$ square lattice EHM discussed in § 3.2.

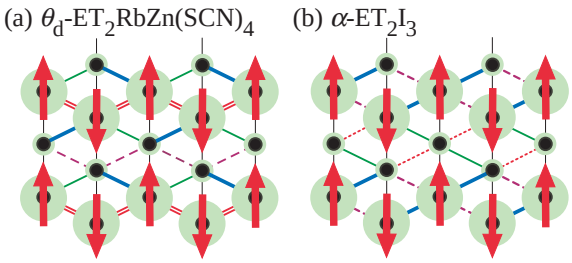

Fig. 16. (Color online) Schematic drawing of mean-field solutions[118] for the horizontal stripe-type charge ordered states in extended Hubbard model on anisotropic triangular lattices for (a) $\theta_{\rm d}$-$ET_2RbZn(SCN)_4$ and (b) α-ET_3I_3. Different "p" bonds are represented by different lines following Fig. 12.

In the region of $V_c \simeq V_p$, first in a study setting $t_{ij} = 0$[135] and recently in a MF study,[136] a solution with a larger periodicity called as the "threefold" state (Fig. 15 (d)), which was not considered in ref. 118, is found to have lower energy than the stripe-type CO states. In this state, the carrier densities on the charge rich and the charge poor sites are $1/2+2\delta$ and $1/2-\delta$, respectively (the $t_{ij} = 0$ study[135] provides the extreme case of $\delta = 1/4$, namely, carrier densities of 1 and 1/4). In this state, the carriers can avoid the occupancy in both neighboring pairs, V_c and V_p, therefore it is stabilized at $V_c \simeq V_p$, compared with the stripe-type CO states which cost loss in either one of these Coulomb repulsion terms. Such a long period state in fact appears as a short range order as found in X-ray scattering measurements[137,138] as diffusive rods (no interlayer coherence), in the conductive states of several members of θ-ET_2X. However these are observed at different 2D wave vectors than in the studies above, which may be resolved by introducing longer range of Coulomb interactions in the EHM.[139] In any case this threefold state is metallic since it is incompatible with the periodicity for quarter-filling, in contrast with the stripe-type CO states which is insulating in the strongly correlated regime, therefore these instabilites should be distinguished.

Many θ-type compounds exhibiting CO undergo a first order phase transition accompanying a structural

transformation to a slightly dimerized structure, typically seen in several members of θ-$ET_2MM'(SCN)_4$:[24] the θ_d-type structure, with a modulated molecular network as shown in Fig. 12. MF calculations[118,136] under such structure with full anisotropy of t_{ij} taken into account, but approximating V_{ij} to be two kinds, V_p and V_c, as in the calculation for the θ-type structure, have been performed. The results suggest that a horizontal stripe-type solution as shown in Fig. 16(a) can have the lowest energy for $V_c \gtrsim V_p$. This is the pattern observed in these compounds, such as in θ-$ET_2RbZn(SCN)_4$ below the metal-insluator transition temperature T_{MI}.[138] Such calculations have been performed by directly adopting the low temperature structure for simplicity, while the importance of the coupling to the lattice have been implied.[4,118,140] It is interesting to start from the high temperature θ-type structure and see whether the structural phase transition to θ_d-type together with the CO transition could be reproduced, which awaits future studies.

As for the α-type structure adopting the values of t_{ij} for α-ET_2I_3, MF calculations[118] show that a horizontal stripe solution (Fig. 16(b)) is more stable than the other solutions in the $V_c \gtrsim V_p$ region, in contrast to the vertical stripe type solution found by Kino and Fukuyama[116] stabilized in the small V_{ij} region. This horizontal stripe pattern is in fact in accordance with the experiments below the metal-insulator CO phase transition temperature in this material.[141] It is noteworthy that, in both this salt and in the θ_d-type ET_2X above, the MF calculations and the experiments agree with each other to a degree of the actual molecules having rich and poor carrier density in their rather complicated unit cells.

Recently, Kobayashi *et al.*[142,143] have extended such MF calculations on this compound, α-ET_2I_3, to parameters under pressure, where a so-called narrow-gap semiconducting state is found by experiments.[144,145] The results show successive transitions from the CO insulating to the CO metallic phase, and then to a phase with a peculiar "zero-gap" state, as a function of pressure. This zero-gap state is characterized by a dispersion of anisotropic Dirac fermions at a wave vector $\boldsymbol{k}^0$, which crosses at the Fermi energy. It is noteworthy that $\boldsymbol{k}^0$ is an incommensurate wave vector due to an "accidential degeneracy"[146] naturally emerging in the band structure of this compound, but not related with the symmetry of the lattice structure. There are attempts[143] to explain the anomalous transport properties observed at high pressures[144,145] based on such framework.

The magnetic properties under the stripe-type CO states can be deduced from such MF results together with the picture mentioned above that we have learned from the 1D cases and the 2D square lattice case. The spin degree of freedom is expected to be described by (quasi-) 1D Heisenberg systems with spins on the charge rich sites along the stripes, then quantum fluctuation may destroy the antiferromagnetic spin order found in MF solutions (see Fig. 16). In fact, such behavior is typically observed in the measurements on θ-$ET_2RbZn(SCN)_4$ and α-ET_2I_3 at ambient pressure, both showing horizontal stripe type CO but absolutely different magnetic behavior. In the former, the CO is realized in the θ_d-type structure, where the MF results show that the bonds between charge rich sites are all equivalent along one kind of bond, $p4$ in Fig. 12 (the double solid bonds in Fig. 16(a)), resulting in a uniform Heisenberg coupling J_{p4} between spins along these stripes. On the other hand, in the latter compound, the horizontal stripe pattern results in an alternation of bonds along the charge rich sites, $p2$ and $p3$ in Fig. 12 (the thick solid and long dashed bonds in Fig. 16(b)), therefore spin singlet formation due to alternating J_{p2} and J_{p3} can be expected. These explain the difference seen in the magnetic susceptibility data: a Bonner-Fischer like low-dimensional localized spin behavior in the former[24] and a prominent spin-gap behavior in the latter.[147] We note that in θ-$ET_2RbZn(SCN)_4$, at lower temperature another phase transition takes place: a spin singlet formation due to the spin-Peierls mechanism along the stripes.[24] This is another experimental fact indicating the validity of describing the magnetic properties under stripe-type CO states as 1D Heisenberg models.

Although such procedure above is helpful in qualitatively understand the experiments, MF calculations cannot accurately describe situations where quantum fluctuations play crucial roles as mentioned in § 2. This is indeed the case for the θ-type structure near $V_c \simeq V_p$, as this is a situation under geometrical frustration introduced in § 2.6. In fact, computations including quantum fluctuation by Merino *et al.*[148] showed that the competition between different CO patterns can lead to a "quantum melting" of CO, which is analogous to the case of the zigzag ladder model mentioned in § 2.6. The ground state phase diagram on the V_c-V_p plane for fixed $U = 10t$ is shown in Fig. 17, which is based on the Drude weight calculations on a $L = 16$ site cluster within the Lanczos ED technique explained in the previous subsection. There, a large metallic phase is stabilized in the region of $V_c \simeq V_p$, as in the 1D case we have seen in Fig. 11. The two different stripe-type CO states are stabilized in the less frustrated regions $V_c \gg V_p$ and $V_c \ll V_p$, which are, in contrast, consistent with the MF studies explained above.[118]

Recently another study for this EHM on the θ-type structure using the variational Monte Carlo method has been performed for much larger systems.[129] In this method, variational states with CO patterns together with correlation effects are assumed and the variational energy is calculated numerically by Monte Carlo sampling.[149] The features in the ED calculations above are reproduced, such as the robust metallic phase along the $V_p \simeq V_c$ line. In this metallic phase, the threefold periodic modulation of charge density is found as in the MF study[136] noted above, which, however, did not fit the $L = 16$ cluster used in the ED study.[148] In the large $V_p \simeq V_c$ region, the threefold modulation is rather strong, which becomes weaker for small $V_p \simeq V_c$. There, different metallic states with stripe-type modulation, i.e., stripe-type CO metallic states, have very close variational energies. This indicates that there is large charge fluctuation[104,148] including the threefold state due to the geometrical frustration.

Combining the above results of different theoretical

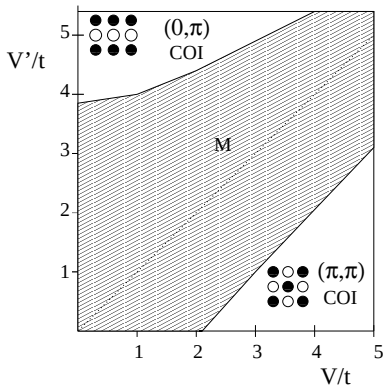

Fig. 17. Lanczos exact diagonalization ground state phase diagram of the quarter-filled extended Hubbard model on the θ-type lattice structure for $U = 10t$.[148] The figure is based on "square lattice" representation: V and V' is respectively equavalent to V_p and V_c in eq. (11), and $t_p = t$, $t_c = 0$. The boundaries are extracted from the Drude weight calculation on a $L = 16$ site cluster. The label M stands for metal, and COI for charge ordered insulator. [Reprinted figure with permission from J. Merino *et al*: Phys. Rev. B **71** (2005) 125111. Copyright (2005) by the American Physical Society.]

methods, one can consider that the horizontal stripe CO states found in the actual θ-ET_2X salts are realized by relaxing the frustration effect through the structural phase transition. In clear contrast, experiments show that members of θ-ET_2X which does not show such structural phase transition are rather conductive, but show a gradual increase of resistivity at low temperatures.[24] There are indications of a glassy CO state in ^{13}C-NMR measurements,[105] which seems to be related with such large charge fluctuation. The additional disorder effect may be responsible for such behavior, which awaits to be understood.

3.4 Superconductivity

Molecular conductors exhibit a variety of SC states as found in quasi-1D Bechgaard salts and quasi-2D ET salts.[6] The issue of their mechanism, particularly the role of spin and charge fluctuations has attracted much attention.[150] When an SDW or an antiferromagnetic phase is located next to the SC phase, it has been often asserted that the spin fluctuation is its origin. As an example, κ-ET_2X shows SC next to an antiferromagnetic Mott insulating phase due to the dimerization.[20] Theoretical calculations for the half-filled Hubbard model on the anisotropic triangular lattice for the κ-type structure show that the SC state here has the $d_{x^2-y^2}$ symmetry mediated by antiferromagnetic spin fluctuation.[151–153] Similarity to the high-T_c cuprates has been discussed,[115] and in fact the d-wave state is stable when the lattice structure is continuously varied from the triangular lattice to the square lattice.[154,155]

On the other hand, recent experiments on 2D A_2B salts suggest the existence of a SC phase in the vicinity of the CO phase, such as in the unified phase diagram of θ-type compounds[24] and SC is actually observed in θ-$(DIETS)_2Au(CN)_4$ under uniaxial pressure.[156] In α-ET_2I_3 under uniaxial pressure, SC is even implied to show up in the presence of CO.[157] These motivated theoretical studies to investigate possibilities of charge fluctuation as an origin of the SC state, based on the 2D EHM on the square lattice as well as on the anisotropic triangular lattice, which we will review in this subsection.

SC mediated by charge fluctuation was discussed first by Scalapino *et al.*[158] for the 3D EHM on the cubic lattice. Relevance of this mechanism to the molecular conductors was pointed out first by Merino and McKenzie,[123] in the quarter-filled square lattice EHM by extending the slave-boson theory for the large-N t-V model[122] introduced in § 3.2. Later several authors[159,160] have extended the weak coupling approach by Scalapino *et al.* (see below) to the square lattice case as well. Their results all show that in the 2D case charge fluctuation due to the nearest-neighbor Coulomb repulsion V can induce a singlet SC state with d_{xy}-wave symmetry.

In the slave-boson theory for the large-N t-V model, the effective interaction $V_{\rm eff}(\boldsymbol{q} = \boldsymbol{k} - \boldsymbol{k}')$, acting between two quasiparticles with momentum $\boldsymbol{k}$ and $-\boldsymbol{k}$ which scatter to $\boldsymbol{k}'$ and $-\boldsymbol{k}'$, can be calculated from the $1/N$ fluctuations around the MF solution at $N \to \infty$.[123,161] As the ratio V/t is increased, the potential varies its shape developing singularities at $(\pm\pi/a, \pm\pi/a)$ toward the critical value $(V/t)_{\rm cr}$ for the occurance of checkerboard CO, at zero temperature (see § 3.2). This leads to an attraction in the channel with d_{xy}-symmetry, and the SC instability is estimated by the coupling averaged over the Fermi surface turning from positive to negative by decreasing temperature.[162] We note that the Fermi surface here has poor nesting, then the pairing mechanism is induced by the intersite Coulomb repulsion V.

The resulting T-V phase diagram is shown in Fig. 18, where the d_{xy}-wave SC state is next to the CO phase discussed in § 3.2, near the critical point $(V/t)_{\rm cr}$. We note that a re-entrant behaviour for the CO phase transition temperature is found, which is also seen in the EHM in infinite dimension using the dynamical MF theory.[163] From the strong coupling viewpoint, the spin fluctuation associated with the fourth order exchange process in eq. (12) couples the next-nearest neighbor sites antiferromagnetically (see Fig. 13). This spin interaction, in turn, cooperates with the charge fluctuation in stabilizing the d_{xy}-wave SC state close to the CO transition.[162]

Search for a SC state near CO in the anisotropic triangular lattice EHM has been pursued by Tanaka *et al.*[164] They used the RPA treatment adopting t_{ij} for θ-$(DIETS)_2[Au(CN)_4]$ as $t_c/t_p = 0.4$, and assumed an isotropic inter-site Coulomb repulsion $V_c = V_p = V$, in eq. (11). In this approximation, the ladder-type diagrams containing V are neglected, but a recent numerical calculation in the fluctuation exchange approximation retaining them[160] showed that the these terms do not change the results qualitatively. The pairing interactions for the singlet and triplet channels are given by

$$V^s(\boldsymbol{q},\omega_l) = U + V(\boldsymbol{q}) + \frac{3}{2}U^2\chi_s(\boldsymbol{q},\omega_l) - (\frac{1}{2}U^2 + 2UV(\boldsymbol{q}) + 2V(\boldsymbol{q})^2)\chi_c(\boldsymbol{q},\omega_l), \quad (18)$$

$$V^t(\boldsymbol{q},\omega_l) = V(\boldsymbol{q}) - \frac{1}{2}U^2\chi_s(\boldsymbol{q},\omega_l)$$

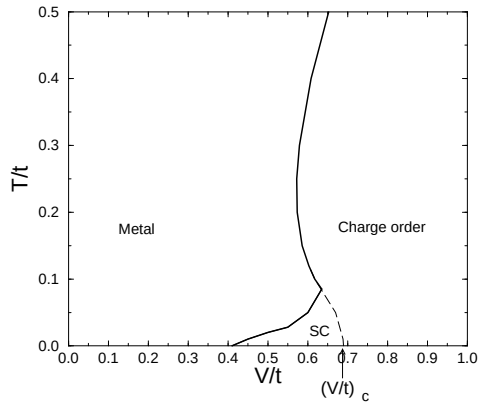

Fig. 18. Phase diagram of the large-N t-V model in the $(T/t,V/t)$ plane showing competition between metallic, superconducting (SC), and charge ordered phases.[123] The symmetry of the Cooper pairs in the superconducting phase is d_{xy}, which is found near the quantum critical point $(V/t)_{\rm cr}$ separating the metallic and charge ordered phases. [Reprinted figure with permission from J. Merino and R. H. McKenzie: Phys. Rev. Lett. **87** (2001) 237002. Copyright (2001) by the American Physical Society.]

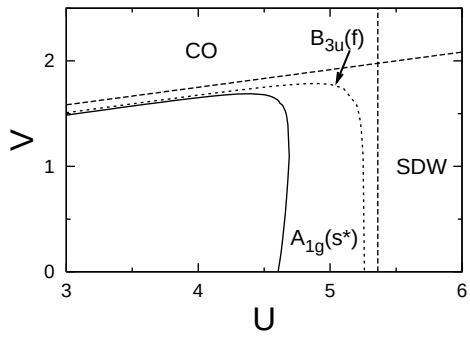

Fig. 19. A weak coupling phase diagram for the quarter-filled extended Hubbard model for the θ-type structure, on the (U,V) plane at $T = 0.01$ (t_p is set as unity and $t_c = 0.4$).[164] The dashed lines correspond to the CO and SDW instabilities. The superconducting order parameter with B_{3u} symmetry is stabilized near the CO instability, although its eigenvalue is slightly smaller than that of the A_{1g} symmetry.

$$-(\frac{1}{2}U^2 + 2UV(\boldsymbol{q}) + 2V(\boldsymbol{q})^2)\chi_c(\boldsymbol{q},\omega_l), \quad (19)$$

respectively, where $V(\boldsymbol{q}) = 2V(\cos q_x + \cos q_y + \cos(q_x + q_y))$ and ω_l is the Matsubara frequency (x and y-directions are taken along the p bonds in Fig. 12). χ_s and χ_c are the spin and charge susceptibilities, respectively. They are calculated within RPA as, $\chi_s(\boldsymbol{q},\omega_l) = \chi_0(\boldsymbol{q},\omega_l)/(1-U\chi_0(\boldsymbol{q},\omega_l))$, $\chi_c(\boldsymbol{q},\omega_l) = \chi_0(\boldsymbol{q},\omega_l)/(1+(U+2V(\boldsymbol{q}))\chi_0(\boldsymbol{q},\omega_l))$, where χ_0 is the bare susceptibility. We note that the terms proportional to χ_c in eqs. (18) and (19) represent effective pairing potentials due to charge fluctuation. This charge fluctuation contributes equally to V^s and to V^t since it comes from the charge degrees of freedom.

To determine the onset of the SC state, the linearized Éliashberg's equation in the weak coupling theory is solved. The obtained phase diagram on the (U,V) plane is shown in Fig. 19 at a fixed temperature $T = 0.01$. $A_{1g}(s^*)$ represents the spin-singlet SC state with A_{1g} symmetry, which is stabilized in the vicinity of both SDW (due to the nesting of Fermi surface) and CO (the three-fold state discussed in § 3.3) instabilities. When $V \simeq 0$, the momentum dependence of the SC order parameter, $\Delta(\boldsymbol{k})$, becomes d_{xy}-like, similarly to the square lattice case.[123, 159, 160]

Near the CO instability, on the other hand, a spin-triplet SC with B_{3u} symmetry is stabilized in addition to the spin-singlet state, although the eigenvalue is slightly smaller than that of the singlet pairing. The momentum dependence of the order parameter $\Delta(\boldsymbol{k})$ shows that it is an f-wave pairing state since it changes the sign six times on the Fermi surface, which is similar to the isotropic triangular lattice case.[165] This SC state is stable because the momentum dependence of V^t gives large attractive interactions at the wave vectors such as $\boldsymbol{Q} = (2\pi/(3a), 2\pi/(3a))$. Actually χ_c has a peak at $\boldsymbol{Q}$ when $(U = 3t_p, V = 1.5t_p)$ leading to a peak in $V^t(\boldsymbol{q})$. We note that, similarly to the square lattice case, this momentum $\boldsymbol{Q}$ is not due to the nesting instability of the noninteracting Fermi surface: $\chi_0(\boldsymbol{q})$ has no notable peak, and $\boldsymbol{Q}$ is determined by the momentum dependence of $V(\boldsymbol{q})$. A recent variational Monte-Carlo calculation[129] have also found the f-wave SC state to be stabilized, which suggests that the SC phase is near but not next to the CO phase.

The stabilities of the d_{xy}-wave pairing in the square lattice and the f-wave pairing in the anisotropic triangular lattice can also be understood from a naive real space picture. The nearest neighbor inter-site Coulomb repulsion repels electrons from the nearest-neighbor sites. The amplitude of the order parameter in real space becomes larger at the four next-nearest-neighbor sites in the square lattice, while in the anisotropic triangular lattice there are six next-nearest-neighbor sites with large amplitude. These corresponds respectively to the d_{xy} and the f-wave pairings.

Let us briefly mention about SC found in α-$(ET)_2I_3$ under uniaxial pressure which appears inside the CO phase; the SC phase transition takes place at a temperature below an upturn of the resistivity is observed, which is probably due to CO.[157] RPA calculations have been performed by Kobayashi *et al.*,[142] based on the reconstructed Fermi surface under the the horizontal stripe-type CO in the metallic phase obtained in the MF results mentioned in 3.3. The results indicate that the SC phase can appear inside the middle CO metallic phase, in which small hole-pockets and electron-pockets both exist.[142] The suggested symmetry of this SC state is s-wave, of which the pairing interaction is mainly given by the spin fluctuation. This implies that in this case the charge fluctuation is suppressed due to the actual existence of CO, and the pairing instability arises from the newly formed Fermi surface.

4. Related Topics

In this section we briefly mention several issues related to CO in A_2B systems that we have discussed. There are many transition metal oxides showing CO whose patterns can be identified as the Wigner-crystal type one. Well known examples are the perovskite type compounds,[166] such as 3D AMO_3 or quasi-2D A_2MO_4

with M being a transition metal. When A is half substituted by another ion with different valence, as $A_{1/2}A'_{1/2}$, M can become mixed valent of half integer, namely, a "quarter"-filled situation is realized. In such cases, an "NaCl"-type CO for the 3D, or the checkerboard-type CO for the quasi-2D compounds is frequently observed. This CO state is actually behind the scene for the well-known collosal magnetoresistance effect (CMR) in perovskite manganites.[167] However, whereas the charge patterns reminds us of the CO states in the molecular systems, the driving force in these systems is usually rather involved. Orbital degeneracy in the d-electron under cubic/tetragonal crystal field, leading to the Jahn-Teller effect which is especially strong for the e_g electron, frequently results in orbital ordering and makes the electronic state highly anisotropic. This together with strong electron correlation give rise to interesting, but at the same time complicated phase diagrams.

Another transition metal oxide compound has been discussed to show a similar CO transition as in the molecular conductors: NaV_2O_5, which has been intensively studied both theoretically as well as experimentally.[168] The transition first found in the magnetic susceptibility,[169] from a behavior of paramagnetic 1D localized spin systems to a spin-gapped state at 35 K, was revealed to be due to the CO transtion.[170] The average valence of the vanadium $V^{4.5+}$ produces a quarter-filled d_{xy}-band, which leads to an effective 2D quarter-filled model. It is the EHM, $\mathcal{H}_{\rm EHM}$ in eq. (1), on the so-called trestle lattice, where two-leg ladders along the a-axis are coupled in a zigzag way along the b-axis. A MF study[110] predicted a CO state with a "zigzag" pattern, which is now confirmed experimentally.[171] As discussed in § 3, such a 2D model is difficult to study in a controlled way, and some authors studied the quarter-filled EHM on a two-leg ladder system.[168,172] In fact, ladders are also found to be realized in molecular systems,[173] which is an interesting target for future studies.

Recently, a triangular lattice system Na_xCoO_2 is attracting interest due to a SC state appearing when intercalated by water, H_2O.[174] At $x = 0.5$, a stripe-type CO state is stabilized, which is discussed to be coupled to the ordering of Na^+ ions.[175] This reminds us of the CO state in θ-$ET_2RbZn(SCN)_4$ where the CO transition couples to the lattice degree of freedom and relaxes the geometrical frustration by lowering the symmetry of the lattice. Similar theoretical approaches to those discussed in this review have been applied to the EHM[176] and the "t-V" model[177] appropriate for this compound.

In the research field of molecular A_2B materials, one important direction of evolution is the inclusion of d-electron spin introduced in the B unit coupled to the organic π-electron on A, the so-called π-d systems.[178] The role of CO here is not clear as it seems that most of such materials are realized in effective half-filled systems such as in the κ- and λ-type structures. It is desired that π-d systems with a quarter-filled π-band would be investigated. It is to be noted that a theoretical work on slightly different molecular system $TPP[FePcCN_2]_2$ (Pc: pentacene), where the $S = 1/2$ Fe^{3+} ion is implanted in the donor π molecule itself, showed that the interaction between localized spins would highly stabilize the CO state and predicted a novel ferromagnetic ground state.[179]

Many different kinds of molecular conductors are continuously and constantly synthesized. We expect that CO states will appear ubiquitously in the new materials as well. Sometimes the effects of CO may be secondary; one recent example is the case of AB_x with x being an incommensurate value close to 1/2, i.e., with an off quarter-filled band. An "incommensurate Mott insulator" has been theoretically proposed,[180] possibly realized in recently synthesized $(MDT\text{-}TS)(AuI_2)_{0.441}$,[181] where the CO instability at quarter-filling indirectly controls the peculiar Mott transition of the system.

5. Summary

To summarize, we have reviewed theoretical studies on charge ordering and related phenomena in the 2:1 charge transfer molecular conductors expressed as A_2B. The charge ordered states are successfully described by extended Hubbard models which starts from the tight-binding model treating the anisotropy carefully enough and consider the electronic correlation, i.e., not only the on-site but also the inter-site Coulomb repulsion, and in some cases with the coupling to the lattice. The physics therein is rich, revealed by considerably numerous amount of studies, but still many issues arise from extensive experiments which anticipate future investigations. Encouraged by this success of understanding the apparently complex system based on constructing microscopic models and treating them by different theoretical techniques, frontiers of research in this field are just about to expand. For example, recent activities on the photo-induced phase transitions in A_2B systems[145,182] requires theoretical efforts with new methods to explore their nonequilibrium dynamics from the microscopic models. Furthermore, there is ambitious proposals[183] to apply our knowledge to even more complex molecular assemblies such as bio-related materials.

Acknowledgments

We would like to acknowledge all of our collaborators in the works on which this review is based on. Especially, we are grateful to H. Fukuyama, A. Greco, R. H. McKenzie, Y. Suzumura, Y. Tanaka, and M. Tsuchiizu for continuous collaborations. We also acknowledge many experimentalists for informative and suggestive discussions. Obviously without these we would not be able to proceed such exciting years of studies.

1) For recent reviews on the field of molecular conductors, Chem. Rev. **104** (2004) 4887-5782.
2) K. Hiraki and K. Kanoda: Phys. Rev. Lett. **80** (1998) 4737.
3) D. S. Chow, F. Zamborszky, B. Alavi, D. J. Tantillo, A. Baur, C. A. Merlic, and S. E. Brown: Phys. Rev. Lett. **85** (2000) 1698.
4) K. Miyagawa, A. Kawamoto, and K. Kanoda: Phys. Rev. B **62** (2000) 7679.
5) J.-P. Farges (ed): *Organic Conductors, Fundamentals and Applications* (Marcel Dekker, New York, 1994).

6) T. Ishiguro, K. Yamaji, and G. Saito: *Organic Superconductors* (Springer-Verlag, Berlin, 1998) 2nd ed.
7) P. Bernier, S. Lefrant, and G. Bidan (eds): *Advances in Synthetic Metals, Twenty Years of Progress in Science and Technology* (Elsevier, Amsterdam, 1999).
8) H. Seo, C. Hotta, and H. Fukuyama: Chem. Rev. **104** (2004) 5005.
9) E. J. W. Verwey and P. W. Haayman: Physica **8** (1941) 979; E. J. W. Verwey, P. W. Haayman, and C. W. Romeijn: J. Chem. Phys. **15** (1947) 181.
10) For recent reviews, N. Tsuda, K. Nasu, A. Fujimori, and K. Shiratori: *Electronic Conduction in Oxides* 2nd ed. (Springer-Verlag, Berlin, 2000), p. 243; F. Walz: J. Phys. Condens. Matter **14** (2002) R285.
11) J. T. Devreese, R. P. Evrard, and V. E. van Doren (eds): *Highly Conducting One-Dimensional Solids* (Plenum, New York, 1979).
12) S. Kagoshima, H. Nagasawa, and T. Sambongi: *One-Dimensional Conductors* (Springer-Verlag, Berlin, 1989).
13) J. Hubbard: Phys. Rev. B **17** (1978) 494.
14) R. Kato, S. Kagoshima, H. Fukuyama, H. Kino, and H. Seo: in ref. 7.
15) R. Hoffman: J. Chem. Phys. **39** (1963) 1397.
16) T. Mori, A. Kobayashi, T. Sasaki, H. Kobayashi, G. Saito, and H. Inokuchi: Bull. Chem. Soc. Jpn. **57** (1984) 627.
17) H. Kino and H. Fukuyama: J. Phys. Soc. Jpn. **65** (1996) 2158.
18) H. Fukuyama, H. Seo, and H. Kino: Physica B **280** (2000) 462; H. Fukuyama and H. Seo: J. Phys. Soc. Jpn. **69** Suppl. B (2000) 144.
19) H. Kino and H. Fukuyama: J. Phys. Soc. Jpn. **64** (1995) 2726.
20) K. Miyagawa, K. Kanoda, and A. Kawamoto: Chem. Rev. **104** (2004) 5635; K. Kanoda: this Volume.
21) T. Itou, K. Kanoda, K. Murata, T. Matsumoto, K. Hiraki, and T. Takahashi: Phys. Rev. Lett. **93** (2004) 216408.
22) W. Yu, F. Zhang, F. Zamborszky, B. Alavi, A. Baur, C. A. Merlic, and S. E. Brown: Phys. Rev. B **70** (2004) 121101.
23) D. Jérome and H. J. Schulz: Adv. Phys. **31** (1982) 299; D. Jérome: Science **252** (1991) 1509; Chem. Rev. **104** (2004) 5565.
24) H. Mori, S. Tanaka, and T. Mori: Phys. Rev. B **57** (1998) 12023.
25) T. Takahashi, K. Yakushi, and Y. Nogami: this Volume.
26) A. A. Ovchinnikov: Sov. Phys. JETP **37** (1973) 176.
27) P. A. Lee, T, M. Rice, and R. A. Klemm: Phys. Rev. B **15** (1977) 2984.
28) J. Kondo and K. Yamaji: J. Phys. Soc. Jpn. **43** (1978) 424.
29) S. Mazumdar and A. N. Bloch: Phys. Rev. Lett. **50** (1983) 207; S. Mazumdar, S. N. Dixit, and A. N. Bloch: Phys. Rev. B **30** (1984) 4842.
30) J. E. Hirsch and D. J. Scalapino: Phys. Rev. Lett. **50** (1983) 1168; Phys. Rev. B **27** (1983) 7169; Phys. Rev. B **29** (1984) 5554.
31) F. Mila and X. Zotos: Europhys. Lett **24** (1993) 133.
32) K. Penc and F. Mila: Phys. Rev. B **49** (1994) 9670.
33) F. Mila: Phys. Rev. B **52** (1995) 4788.
34) C. S. Jacobsen: J. Phys. C **19** (1986) 5643.
35) H. Seo and H. Fukuyama: J. Phys. Soc. Jpn. **66** (1997) 1249.
36) T. Nakamura, T. Nobutoki, Y. Kobayashi, T. Takahashi, and G. Saito: Synth. Met. **70** (1995) 1293.
37) P. Monceau, F.Ya. Nad, and S. Brazovskii: Phys. Rev. Lett. **86** (2001) 4080.
38) For a review, S. Hünig and E. Herberth: Chem. Rev. **104** (2004) 5535.
39) K. Hiraki and K. Kanoda: Phys. Rev. B **54** (1996) 17276.
40) Y. Kashimura, H. Sawa, S. Aonuma, R. Kato, H. Takahashi, and N. Môri: Solid State Commun. **93** (1995) 675; R. Kato, H. Kobayashi, and A. Kobayashi: J. Am. Chem. Soc. **111** (1989) 5224.
41) T. Miyazaki and K. Terakura: Phys. Rev. B **54** (1996) 10452.
42) T. Mori, A. Kobayashi, Y. Sasaki, and H. Kobayashi: Chem. Lett. **1982** (1982) 1923.
43) P. M. Grant: J. de Phys. **44** (1983) C3-847.
44) L. Ducasse, M. Abderrabba, J. Hoarau, M. Pesquer, B. Gallois, and J. Gaultier: J. Phys. C **19** (1986) 3805.
45) T. Mori: Bull. Chem. Soc. Jpn. **71** (1998) 2509; T. Mori, H. Mori, and S. Tanaka: Bull. Chem. Soc. Jpn. **72** (1999) 179; T. Mori: Bull. Chem. Soc. Jpn. **72** (1999) 2011.
46) A. Fritsch and L. Ducasse: J. Phys. I France **1** (1991) 855.
47) F. Castet, A. Fritsch, and L. Ducasse: J. Phys. I France **6** (1996) 583.
48) Y. Imamura, S. Ten-no, K. Yonemitsu, and Y. Tanimura: Chem. Phys. Lett. **298** (1998) 15.
49) For example, K. Kishigi and Y. Hasegawa: J. Phys. Soc. Jpn. **69** (2000) 2145; Y. Tomio and Y. Suzumura: J. Phys. Chem. Solids **62** (2001) 431; H. Yoshioka: to be published in J. Phys. Soc. Jpn. **75** (2006) No.3 (condmat/0511150).
50) For example, see J. P. Pouget and S. Ravy: J. Phys. I France **6** (1996) 1501; S. Ravy: Chem. Rev. **104** (2004) 5609.
51) C. N. Yang and C. P. Yang: Phys. Rev. **150** (1966) 321; Phys. Rev. **150** (1966) 327.
52) P. W. Anderson: Phys. Rev. **102** (1956) 1008.
53) Y. Tanaka and M. Ogata: J. Phys. Soc. Jpn. **74** (2005) 3283.
54) M. Ogata and H. Shiba: Phys. Rev. B **41** (1990) 2326.
55) H. Shiba and M. Ogata: Int. J. Mod. Phys. B **5** (1991) 31.
56) Z. L. Berezinskii: Sov. Phys. JETP **32** (1971) 493; Sov. Phys. JETP **34** (1972) 610.
57) J. M. Kosterlitz and D. J. Thouless: J. Phys. C **6** (1973) 1181; J. M. Kosterlitz: J. Phys. C **7** (1974) 1046.
58) J. des Cloizeaux and M. Gaudin: J. Math. Phys. **7** (1966) 1384.
59) For example, see E. Dagotto: Rev. Mod. Phys. **66** (1994) 763, and references therein.
60) K. Sano and Y. Ōno: J. Phys. Soc. Jpn. **63** (1994) 1250; Phys. Rev. B **70** (2004) 155102.
61) M. Nakamura, A. Kitazawa, and K. Nomura: Phys. Rev. B **60** (1999) 7850; M. Nakamura: Phys. Rev. B **61** (2000) 16377.
62) R. T. Clay, S. Mazumdar, and D. K. Campbell: Phys. Rev. B **67** (2003) 115121.
63) S. Ejima, F. Gebhard, and S. Nishimoto: Europhys. Lett **70** (2005) 492.
64) M. Ogata, M. U. Luchini, S. Sorella, and F. F. Assaad: Phys. Rev. Lett. **66** (1991) 2388.
65) For a review, F. Mila and K. Penc: J. Electron Spectrosc. Relat. Phenom. **117-118** (2001) 451.
66) J. Bernasconi, M. J. Rice, W. R. Schneider, and S. Strässler: Phys. Rev. B **12** (1975) 1090.
67) K. Penc and F. Mila: Phys. Rev. B **50** (1994) 11429.
68) V. J. Emery, R. Bruisma, and S. Barišić: Phys. Rev. Lett. **48** (1982) 1038.
69) S. Nishimoto, M. Takahashi, and Y. Ohta: J. Phys. Soc. Jpn. **69** (2000) 1594.
70) Y. Shibata, S. Nishimoto, and Y. Ohta: Phys. Rev. B **64** (2001) 235107.
71) H. Otsuka and M. Nakamura: Phys. Rev. B **70** (2004) 073105.
72) For recent reviews, J. Viot: Rep. Prog. Phys. **57** (1994) 977; T. Giamarchi: *Quantum Physics in One Dimension* (Oxford University Press, 2004).
73) H. Yoshioka, M. Tsuchiizu, and Y. Suzumura: J. Phys. Soc. Jpn. **69** (2000) 651.
74) H. Yoshioka, M. Tsuchiizu, and Y. Suzumura: J. Phys. Soc. Jpn. **70** (2001) 762.
75) T. Giamarchi and A. J. Millis: Phys. Rev. B **46** (1992) 9325.
76) H. J. Schulz: in *Strongly Correlated Electronic Materials*, eds. K. S. Bedell, Z. Wang, D. E. Meltzer, A. V. Balatsky, and E. Abraham (Addison-Wesley Publish Company, 1994).
77) T. Giamarchi: Physica B **230-232** (1997) 975.
78) K. Yonemitsu: Phys. Rev. B **56** (1997) 7262.
79) H. Fukuyama and H. Takayama: in *Electronic Properties of Inorganic Quasi-One-Dimensional Compounds*, ed. P. Monceau (D. Reidel Publishing Company, Dordrecht/Boston/Lancaster, 1985), p.41.
80) M. Tsuchiizu, H. Yoshioka, and Y. Suzumura: J. Phys. Soc. Jpn. **70** (2001) 1460.
81) M. Tsuchiizu and E. Orignac: J. Phys. Chem. Solids **63** (2002) 1459.
82) For a review, J. Kishine and K. Yonemitsu: Int. J. Mod. Phys.

B **16** (2002) 711.
83) H. Yoshioka, M. Tsuchiizu, and H. Seo: in preparation.
84) D. J. Scalapino, Y. Imry, and P. Pincus: Phys. Rev. B **11** (1975) 2042.
85) J. W. Bray, L. V. Interrante, I. S. Jacobs, and J. C. Bonner: in *Extended Linear Compounds Vol. 3*, ed. J. C. Miller (Plenum, New York, 1983), p. 353.
86) H. Fukuyama and S. Inagaki: in *Magnetic Properties of Low-Dimensional Systems*, ed. L. M. Falikov and J. L. Morán-López (Springer-Verlag, Berlin, 1986), p. 156.
87) S. Robaszkiewicz and T. Kostyrko: Physica **121B** (1983) 134.
88) P. P. Bendt: Phys. Rev. B **30** (1984) 3951.
89) K. C. Ung, S. Mazumdar, and D. Toussaint: Phys. Rev. Lett. **73** (1994) 2603.
90) J. Riera and D. Poilblanc: Phys. Rev. B **62** (2000) 16243.
91) M. Kuwabara, H. Seo, and M. Ogata: J. Phys. Soc. Jpn. **72** (2003) 225.
92) M. Sugiura and Y. Suzumura: J. Phys. Soc. Jpn. **72** (2003) 1458; M. Sugiura, M. Tsuchiizu, and Y. Suzumura: J. Phys. Soc. Jpn. **73** (2004) 2487; J. Phys. Soc. Jpn. **74** (2005) 983.
93) For example, see Chapter 8.3 in ref. 6.
94) A. Ota, H. Yamochi, and G. Saito: J. Mater. Chem. **12** (2002) 2600.
95) O. Drozdova, K. Yakushi, K. Yamamoto, A. Ota, H. Yamochi, G. Saito, H. Tashiro, and D. B. Tanner: Phys. Rev. B **70** (2004) 075107.
96) J. Riera and D. Poilblanc: Phys. Rev. B **63** (2001) 241102.
97) H. Seo, T. Kato, and Y. Motome: in preparation.
98) A. P. Ramirez: in *Handbook of Magnetic Materials*, ed. K. H. J. Buschow (Elsevier, Amsterdam, 2001), Vol. 13, p. 423.
99) N. Kobayashi, M. Ogata, and K. Yonemitsu: J. Phys. Soc. Jpn. **67** (1998) 1098.
100) H. Seo and M. Ogata: Phys. Rev. B **64** (2001) 113103.
101) S. Nishimoto and Y. Ohta: Phys. Rev. B **68** (2003) 235114.
102) V. J. Emery and C. Noguera: Phys. Rev. Lett. **60** (1988) 631.
103) S. Ejima, F. Gebhard, S. Nishimoto, and Y. Ohta: Phys. Rev. B **72** (2005) 033101.
104) H. Seo, K. Tsutsui, M. Ogata, and J. Merino: in preparation.
105) K. Kanoda, K. Ohnou, M. Kodama, K. Miyagawa, T. Itou, and K. Hiraki: J. de Physique IV **131** (2005) 21.
106) R. Tazaki *et al.*, private communications.
107) R. Kato: Bull. Chem. Soc. Jpn. **73**, 515 (2000).
108) For a review, E. W. Carlson, V. J. Emery, S. A. Kivelson, and D. Orgad: in *The Physics of Superconductors, Vol. 2*, ed. K. H. Bennemann and J. B. Ketterson (Springer-Verlag, 2004) (cond-mat/0206217).
109) Y. Ohta, K. Tsusui, W. Koshibae, and S. Maekawa: Phys. Rev. B **50** (1994) 13594.
110) H. Seo and H. Fukuyama: J. Phys. Soc. Jpn. **67** (1998) 2602.
111) R. Chiba, H. M. Yamamoto, T. Nakamura, and T. Takahashi: J. Phys. Chem. Solids **62** (2001) 389.
112) Y. Takano, K. Hiraki, H. M. Yamamoto, T. Nakamura, and T. Takahashi: J. Phys. Chem. Solids **62** (2001) 393.
113) H. Kino and H. Fukuyama: J. Phys. Soc. Jpn. **64** (1995) 4523.
114) C. Hotta: J. Phys. Soc. Jpn. **72** (2003) 840; C. Hotta and H. Fukuyama: J. Phys. Soc. Jpn. **70** (2001) 321.
115) R. H. McKenzie: Science **278** (1997) 820; Comments Condens. Matter Phys. **18** (1998) 309.
116) H. Kino and H. Fukuyama: J. Phys. Soc. Jpn. **64** (1995) 1877.
117) H. Seo and H. Fukuyama: J. Phys. Soc. Jpn. **67** (1998) 1848.
118) H. Seo: J. Phys. Soc. Jpn. **69** (2000) 805.
119) L. Ducasse, A. Fritsch, and F. Castet: Synth. Met. **85** (1997) 1627.
120) Y. Imamura, S. Ten-no, K. Yonemitsu, and Y. Tanimura: J. Chem. Phys. **111** (1999) 5986.
121) T. Mori: Bull. Chem. Soc. Jpn. **73** (2000) 2243.
122) R. H. McKenzie, J. Merino, J. B. Marston, and O. P. Sushkov: Phys. Rev. B **64** (2001) 085109.
123) J. Merino and R. H. McKenzie: Phys. Rev. Lett. **87** (2001) 237002.
124) E. Manousakis: Rev. Mod. Phys. **63** (1991) 1.
125) M. Calandra, J. Merino, and R. H. McKenzie: Phys. Rev. B **66** (2002) 195102.
126) W. Kohn: Phys. Rev. **133** (1964) A171.
127) W. Stephan and P. Horsch: Phys. Rev. B **42** (1990) 8736.
128) D. J. Scalapino, S. R. White, and S. Zhang: Phys. Rev. B **47** (1993) 7995.
129) H. Watanabe and M. Ogata: preprint (cond-mat/0602536).
130) K. Hanasaki and M. Imada: J. Phys. Soc. Jpn. **76** (2005) 2769.
131) For a review on the use in heavy fermion problems, D. M. Newns and N. Read: Adv. Phys. **36** (1987) 799.
132) G. Kotliar and A. E. Ruckenstein: Phys. Rev. Lett. **57** (1986) 1362; G. Kotliar and J. Liu: Phys. Rev. Lett. **61** (1988) 1784.
133) K. Yakushi, K. Yamamoto, M. Simonyan, J. Ouyang, C. Nakano, Y. Misaki, and K. Tanaka: Phys. Rev. B **66** (2002) 235102.
134) K. Suzuki, K. Yamamoto, and K. Yakushi: Phys. Rev. B **69** (2004) 085114.
135) T. Mori: J. Phys. Soc. Jpn. **72** (2003) 1469.
136) M. Kaneko and M. Ogata:J. Phys. Soc. Jpn. **75** (2006) 014710.
137) M. Watanabe, Y. Nogami, K. Oshima, H. Mori, and S. Tanaka: J. Phys. Soc. Jpn. **68** (1999) 2654.
138) M. Watanabe, Y. Noda, Y. Nogami, and H. Mori: J. Phys. Soc. Jpn. **73** (2004) 116; J. Phys. Soc. Jpn. **74** (2005) 2011.
139) K. Kuroki: private communications.
140) R. T. Clay, S. Mazumdar, and D. K. Campbell: J. Phys. Soc. Jpn. **71** (2002) 1816.
141) T. Kakiuchi *et al.*: private communications.
142) A. Kobayashi, S. Katayama and Y. Suzumura: J. Phys. Soc. Jpn. **74** (2005) 2987.
143) S. Katayama, A. Kobayashi, and Y. Suzumura: J. Phys. Soc. Jpn. **75** (2006) 023708; cond-mat/0601068.
144) N. Tajima, M. Tamura, Y. Nishio, K. Kajita and Y. Iye: J. Phys. Soc. Jpn. **69** (2000) 543.
145) N. Tajima, R. Kato, and K. Kajita: this volume.
146) C. Herring: Phys. Rev. **52** (1937) 365.
147) B. Rothamael, L. Forro, J. R. Cooper, J. S. Schilling, M. Weger, P. Bele, H. Brunner, D. Schweitzner, and H. J. Keller: Phys. Rev. B **34** (1986) 704.
148) J. Merino, H. Seo, and M. Ogata: Phys. Rev. B **71** (2005) 125111.
149) For example, see H. Yokoyama and H. Shiba, J. Phys. Soc. Jpn. **56** (1987) 1490.
150) K. Kuroki: this volume.
151) H. Kino and H. Kontani: J. Phys. Soc. Jpn. **67** (1998) 3691.
152) J. Schmalian: Phys. Rev. Lett. **81** (1998) 4232.
153) H. Kondo and T. Moriya: J. Phys. Soc. Jpn. **67** (1998) 3695.
154) M. Ogata: J. Phys. Soc. Jpn. **72** (2003) 1839.
155) H. Kontani: Phys. Rev. B **67** (2003) 180503(R).
156) N. Tajima, T. Imakubo, R. Kato, Y. Nishio, and K. Kajita: J. Phys. Soc. Jpn. **72** (2003) 1014.
157) N. Tajima, A. Ebina-Tajima, M. Tamura, Y. Nishio, and K. Kajita: J. Phys. Soc. Jpn. **71** (2002) 1832.
158) D. J. Scalapino, E. Loh, Jr., and J. E. Hirsch: Phys. Rev. B **35** (1987) 6694.
159) A. Kobayashi, Y. Tanaka, M. Ogata, and Y. Suzumura: J. Phys. Soc. Jpn. **73** (2004) 1115.
160) S. Onari, R. Arita, K. Kuroki, and H. Aoki: Phys. Rev. B **70** (2004) 094523.
161) J. Merino, A. Greco, R. H. McKenzie, and M. Calandra: Phys. Rev. B **68** (2003) 245121.
162) A. Greco, J. Merino, A. Foussats, and R. H. McKenzie: Phys. Rev. B **71** (2005) 144502.
163) R. Pietig, R. Bulla, and S. Blawid: Phys. Rev. Lett. **82** (1999) 4046.
164) Y. Tanaka, Y. Yanase, and M. Ogata: J. Phys. Soc. Jpn. **73** (2004) 2053.
165) Y. Tanaka, Y. Yanase, and M. Ogata: J. Phys. Soc. Jpn. **73** (2004) 319.
166) For a review, M. Imada, A. Fujimori, and Y. Tokura: Rev. Mod. Phys. **70** (1998) 1039.
167) For a review, Y. Tokura and N. Nagaosa: Science **288** (2000) 462.
168) For a review, P. Lemmens, G. Guntherodt, and C. Gros: Phys. Rep. **375** (2003) 1.
169) M. Isobe and Y. Ueda: J. Phys. Soc. Jpn. **65** (1996) 1178.

170) T. Ohama, H. Yasuoka, M. Isobe, and Y. Ueda: Phys. Rev. B **59** (1999) 3299.
171) K. Ohwada, Y. Fujii, Y. Katsuki, J. Muraoka, H. Nakao, Y. Murakami, H. Sawa, E. Ninomiya, M. Isobe, and Y. Ueda: Phys. Rev. Lett. **94** (2005) 106401, and references therein.
172) M. Vojta, A. Hübsch, and R. M. Noack: Phys. Rev. B **63** (2001) 45105.
173) For a review, C. Rovira: Chem. Eur. J. **6** (2000) 1723.
174) K. Takada, H. Sakurai, E. Takayama-Muromachi, F. Izumi, R. A. Dilanian, and T. Sasaki: Nature (London) **422** (2003) 53.
175) M. L. Foo, Y. Wang, S. Watauchi, H. W. Zandbergen, T. He, R. J. Cava, and N. P. Ong: Phys. Rev. Lett. **92** (2004) 247001.
176) H. Watanabe and M. Ogata: J. Phys. Soc. Jpn. **74** (2005) 2901.
177) O. I. Motrunich and P. A. Lee: Phys. Rev. B **69** (2004) 214516; Phys. Rev. B **70** (2004) 024514.
178) H. Kobayashi and A. Kobayashi: this volume.
179) C. Hotta, M. Ogata, and H. Fukuyama: Phys. Rev. Lett. **95** (2005) 216402.
180) H. Yoshioka, H. Seo, and H. Fukuyama: J. Phys. Soc. Jpn. **74** (2005) 1922.
181) K. Takimiya, M. Kodani, N. Niihara, Y. Aso, T. Otsubo, Y. Bando, T. Kawamoto, and T. Mori: Chem. Mater. **16** (2004) 5120; T. Kawamoto, Y. Bando, T. Mori, K. Takimiya , and T. Otsubo: Phys. Rev. B **71** (2005) 052501.
182) M. Chollet, L. Guerin, N. Uchida, S. Fukaya, H. Shimoda, T. Ishikawa, K. Matsuda, T. Hasegawa, A. Ota, H. Yamochi, G. Saito, R. Tazaki, S. Adachi, and S. Koshihara: Sceince **307** (2005) 86.
183) H. Fukuyama: this volume.